



TAMPEREEN TEKNILLINEN YLIOPISTO  
TAMPERE UNIVERSITY OF TECHNOLOGY

ANNE HAAPALA  
POROUS POLY(BUTYLENE SUCCINATE) FILMS AS PROMISING  
CANDIDATES FOR RETINAL TISSUE ENGINEERING

Master of Science Thesis

Examiner: Professor Minna  
Kellomäki, Dr. Teresa Rebelo Calejo  
Examiner and topic approved by the  
Faculty Council of the Faculty of Nat-  
ural Sciences on 31st October 2018

## ABSTRACT

**ANNE HAAPALA:** Porous poly(butylene succinate) films as promising candidates for retinal tissue engineering

Tampere University of technology

Master of Science Thesis, 68 pages

December 2018

Master's Degree Programme in Biotechnology

Major: Tissue Engineering

Examiner: Professor Minna Kellomäki, Dr. Teresa Rebelo Calejo

**Keywords:** Poly(butylene succinate), retina, tissue engineering, scaffold, porous thin film, honeycomb, breath figure, particulate leaching, pluripotent stem cells

In the developed world, degenerative retinal diseases such as age-related macular degeneration (AMD) are the leading cause of senior citizens' vision loss. AMD is caused by the degeneration of the retinal pigment epithelium (RPE), hence RPE transplantation is considered the most promising solution for reversing the degeneration and vision loss.

The purpose of this study was to develop biodegradable scaffolds that have similar properties as the natural Bruch's membrane (BM) and to study the cell adhesion on them. Particulate leaching (PL) and breath figure (BF) method were used to prepare porous films from poly(butylene succinate) (PBSu). These films were characterized by their thickness, surface porosity and pore size, hydrophilicity, roughness, diffusion properties as well as their degradation behaviour. Films with honeycomb (HC) structured surface were able to be prepared with the BF method by using 1,2-dioleoyl-sn-glycero-3-phosphoethanolamine (DOPE) as a surfactant. These films were also found to be much more hydrophilic than any of the other films created without surfactant. Films prepared by the PL method with sucrose particles also showed a slightly higher hydrophilicity than the control films without sucrose or surfactant, but the pores on these films were not as organized and evident as on the honeycomb films created with the BF method.

In this work, human embryonic stem cell-derived retinal pigment epithelium (hESC-RPE) cell adhesion to porous PBSu films is studied for the first time. Cell culture studies using hESC-RPE cells showed good cell adhesion and protein secretion on the collagen IV and laminin dip-coated films, while there were barely any cells adhered to the uncoated films. The cells expressed elongated fibroblast like shape on films prepared by the PL method, while the HC structured films prepared by the BF method and commercial polyethylene terephthalate (PET) films used as controls, helped cells to maintain a more rounded shape, typical to RPE cells. This study demonstrates the potential of porous PBSu scaffolds as prosthetic BMs for tissue engineering of hESC-RPE.

## TIIVISTELMÄ

**ANNE HAAPALA:** Porous poly(butylene succinate) films as promising candidates for retinal tissue engineering

Tampereen teknillinen yliopisto

Diplomityö, 68 sivua

Joulukuu 2018

Biotekniikan diplomi-insinöörin tutkinto-ohjelma

Pääaine: Kudosteknologia

Tarkastaja: Professori Minna Kellomäki, Dr. Teresa Rebelo Calejo

**Avainsanat:** Polybutyleeni sukkinatti, verkkokalvo, kudosteknologia, skaffoldi, huokoinen kalvo, hunajakanno, pluripotentti kantasolu

Verkkokalvon rappeumasairaudet kuten verkkokalvon ikärappeuma ovat yleisimmät syyt vanhempien ihmisten sokeutumiseen länsimaissa. Verkkokalvon ikärappeuma johtuu peruuttamattomista vaurioista verkkokalvon pigmenttiepiteelin (RPE) toiminnassa. Tästä syystä vaurioituneiden RPE-solujen korvaamista terveillä soluilla pidetään mahdollisena verkkokalvon rappeumasairauksien hoitokeinona.

Tämän diplomityön tavoitteena oli valmistaa biohajoavia skaffoldeja, jotka muistuttavat ominaisuuksiltaan luonnollista Bruchin kalvoa, ja tutkia niiden soveltuvuutta RPE-solujen viljelyyn. Huokoisia kalvoja valmistettiin partikkelien liuotusmenetelmällä (PL-menetelmä) ja breath figure (BF)-menetelmällä polybutyleeni sukkinatista (PBSu). Näillä tavoin valmistettujen kalvojen soveltuvuutta verkkokalvoskaffoldeiksi analysoitiin niiden paksuuden, huokoisuuden, huokoskoon, pinnan karkeuden sekä biohajoamisominaisuuksien perusteella. BF-menetelmällä saatiin aikaan kalvoja, joissa oli hunajakennomainen pintarakenne, ja näiden havaittiin myös olevan huomattavasti muita kalvoja hydrofiilisempiä. PL-menetelmällä sukroosipartikkelien avulla valmistetut kalvot olivat myös hieman hydrofiilisempia kuin samoilla menetelmillä valmistetut kontrollikalvot. Nämä kalvot eivät kuitenkaan omanneet yhtä huokoista pintarakennetta kuin BF-menetelmällä valmistetut hunajakennomaiset kalvot.

Tämä työ on ensimmäinen, jossa tutkittiin ihmisen alkion kantasoluista erilaistettujen RPE (hESC-RPE)-solujen kiinnittymistä huokoisten PBSu kalvojen pinnalle. hESC-RPE-solut kiinnittyivät hyvin kollageenilla ja laminiinilla pinnoitettuihin kalvoihin, ja ne erittivät myös huomattavasti vinkuliinia, aktiinia, kollageenia, laminiinia ja fibronectiinia. Toisaalta solut eivät juurikaan kiinnittyneet ja kasvaneet kalvoilla ilman proteiinipinnoitetta. Solut ilmensivät pitkänomaista, fibroblastia muistuttavaa muotoa PL-menetelmällä valmistetuilla kalvoilla. Hunajakennomaisilla kalvoilla, ja kontrollina käytetyillä kaupallisilla polyeteeni tereftalaattikalvoilla (PET) solut puolestaan säilyttivät RPE soluille tyypillisen pyöreämmän muodon. Tämä tutkimus havainnollistaa huokoisten PBSu skaffoldien potentiaalia toimia keinotekoisena Bruchin kalvona hESC-RPE-solujen implantoinnissa

## PREFACE

This study was done as a collaboration between the Eye Regeneration Group of the Institute of Biosciences and Medical Technology (BioMediTech) at University of Tampere and the Biomaterials Science and Tissue Engineering Group of Tampere University of Technology.

Firstly, I would like to thank Professor Minna Kellomäki and Professor Heli Skottman for providing me such an interesting topic for my thesis. I would also like to thank my supervisor Teresa Rebelo Calejo PhD for giving me guidance throughout the thesis process and for always being ready to help me with any problems I had. I could not have done this without your help. Moreover, I would like to thank everyone in Eye Regeneration Group as well as Biomaterials Science and Tissue Engineering Group who gave me a hand during the work.

Finally, a huge thank you to my family and friends for always supporting me and being there for me no matter what, especially my parents. You have kept me going all these years. Special thanks also to my oz brother Fin for proofreading my thesis, I owe you big time.

CERN, 21.11.2018

Anne Haapala

## CONTENTS

1.	INTRODUCTION .....	1
2.	LITERATURE REVIEW .....	3
	2.1 Poly(butylene succinate) .....	3
	2.1.1 Properties.....	4
	2.1.2 Biodegradation .....	5
	2.1.3 PBSu in tissue engineering.....	6
	2.2 Methods for film manufacturing .....	7
	2.2.1 Particulate leaching .....	7
	2.2.2 Breath figure method.....	9
	2.3 Retina .....	10
	2.3.1 Retinal pigment epithelium .....	11
	2.3.2 Retinal pigment epithelium function.....	11
	2.3.3 Bruch's membrane .....	12
	2.3.4 Age-related macular degeneration .....	13
	2.3.5 Human embryonic stem cell-derived RPE .....	13
	2.3.6 Cell adhesion .....	14
3.	MATERIALS AND METHODS.....	17
	3.1 Film preparation .....	17
	3.1.1 Solvent casting .....	17
	3.1.2 Particulate leaching .....	18
	3.1.3 Breath figure method.....	20
	3.2 Film characterization.....	21
	3.2.1 Macroscopic and microscopic features .....	21
	3.2.2 Determination of film thickness .....	22
	3.2.3 Water contact angle .....	22
	3.2.4 Electrical resistance.....	22
	3.2.5 <i>In vitro</i> stability of PBSu films .....	22
	3.3 Cell culture .....	23
	3.3.1 Disinfecting the membranes.....	23
	3.3.2 Coating the membranes .....	23
	3.3.3 Culturing the cells .....	24
	3.3.4 Cell viability.....	24
	3.3.5 Immunostainings .....	25
	3.4 Confocal microscopy.....	27
4.	RESULTS AND DISCUSSION .....	28
	4.1 Film characterization.....	28
	4.1.1 Film thickness .....	28
	4.1.2 Surface structure and porosity.....	32
	4.1.3 <i>In vitro</i> stability of PBSu films .....	36
	4.1.4 Film wettability .....	42

4.1.5 Electrical resistance .....	44
4.2 Cell culture .....	45
4.2.1 Cell viability .....	46
4.2.2 Immunostaining .....	47
5. CONCLUSIONS .....	56
6. REFERENCES .....	58

## LIST OF SYMBOLS AND ABBREVIATIONS

$m_0$	The initial mass of the film
$m_f$	The final dry mass of the film
$m_{f,wet}$	The final wet mass of the film.
AFM	Atomic force microscope
AMD	Age-related macular degeneration
BD	1,4-butanediol
BF	Breath figure
bFGF	Basic fibroblast growth factor
BM	Bruch's membrane
BRB	Blood retinal barrier
BSA	Bovine serum albumin protein
CaCl <sub>2</sub>	Calcium chloride
CO <sub>2</sub>	Carbon dioxide
DAPI	4',6'-diamidino-2-phenylidole
DOPE	1,2-dioleoyl-sn-glycero-3-phosphoethanolamine
DPBS	Dulbecco's phosphate-buffered saline
ECM	Extracellular matrix
FA	Focal adhesion
FITC	Fluorescein isothiocyanate
HC	Honeycomb
HDPE	High-density polyethylene
hESC	Human embryonic stem cell
hESC-RPE	Human embryonic stem cell-derived RPE
hMSC	Human mesenchymal stem cells
IF	Immunofluorescence
LDPE	Low-density polyethylene
MgCl <sub>2</sub>	Magnesium chloride
MC3T3-E1	Mouse calvaria-derived pre-osteoblastic cells
NaCl	Sodium chloride
NaOH	Sodium hydroxide
PBS	Phosphate-buffered saline
PBSu	Poly(butylene succinate)
PCL	Poly( $\epsilon$ -caprolactone)
PE	Polyethylene
PET	Polyethylene terephthalate
Phalloidin	Phalloidin-tetramethylrhodamine B isothiocyanate
PL	Particulate leaching
PLA	Poly(lactide)
PLCL	Poly(L-lactide-co- $\epsilon$ -caprolactone)
PLDLA	Poly(L-D-lactide)
PLGA	Poly(lactide-co-glycolide)
POS	Photoreceptor outer segments
PP	Polypropylene
PSC	Pluripotent stem cell
PTES	Poly(triethylene succinate)
$R_a$	Arithmetic mean of surface roughness
RGD	Arg-Gly-Asp

RH	Relative humidity
RPE	Retinal pigment epithelium
SA	Succinate acid
WCA	Water contact angle

# 1. INTRODUCTION

Age-related macular degeneration (AMD) is a neurodegenerative disease that is mostly caused by progressive degeneration and death of retinal pigment epithelium (RPE) cells at the macula (Kaarniranta et al. 2013). Even though AMD is the leading cause of central blindness in developed countries and is expected to affect 196 million people worldwide by 2020 (Wong et al. 2014), there are still not many effective treatment options available (Riera et al. 2016). Cell therapies, especially studies with pluripotent stem cells (PSCs) differentiating into functional RPE cells, have become the main focus in the field of regenerative medicine, since they appear to be the most promising solution for reversing degeneration and vision loss. (Riera et al. 2016)

RPE is a highly specialized and pigmented cell monolayer that is located between the photoreceptors and Bruch's membrane (BM) in the retina. The RPE cells play an important role in maintaining the survival and functionality of the photoreceptor cells by secreting growth factors, recycling and metabolizing retinoids, transporting nutrients and waste products into and out of the retina, as well as phagocytosing the outer segments of the photoreceptors. (Kaarniranta et al. 2013)

The microenvironment surrounding the cells in tissues affects the cell survival and function. (Barthes et al. 2014) Thus, reproducing the natural environment of RPE cells is vital for human embryonic stem cell-derived RPE (hESC-RPE) cell maturation and function. (Hotaling et al. 2016) Cell therapies with and without the support of a biomaterial scaffold have been studied. For example, transplanting hESC-RPE cells in a suspension to the subretinal space has shown lower cell survival compared to those transplanted as a monolayer on top of a supportive biomaterial membrane. (Diniz et al. 2013) The problem with these biomaterials currently used as a membrane *in vivo* and *in vitro* is that they still do not mimic the natural RPE environment, which could affect the function of the transplanted cells (McCarthy et al. 1996). The natural RPE extracellular matrix (ECM) contains fibrous proteins with nano- and micro-scale features that give topographical stimuli that can influence the cell morphology, movement, function and adhesion (Janson & Putnam 2015). Studies on the effect of material surface properties on cell behavior are therefore needed.

The RPE cell adhesion on different surfaces has been studied, but these studies have mostly used cells from non-human origin, human primary cells or immortalized cell lines as the source of RPE (Singhal & Vemuganti 2005; Shadforth et al. 2012; Shang et al. 2018), while there is limited information available concerning the hESC-RPE adhesion, particularly onto biodegradable and patterned surfaces.

The purpose of this study was to develop biodegradable porous scaffolds from poly(butylene succinate) (PBSu) for tissue engineering of the RPE that enable the flow of molecules, which is essential when the implant is transplanted. The goal was to establish how the different material properties such as surface topography influence the hESC-RPE adhesion and behaviour.



The second step, transesterification (Figure 1b), is conducted under reduced pressure and at higher temperature in order to remove BD. This step also requires a catalyst, for example titanium(IV)butoxide (Gigli et al. 2016).

### 2.1.1 Properties

Table 1 shows the basic properties of PBSu (BIONOLLE) compared to polyolefins such as polypropylene (PP) and high and low-density polyethylene (HDPE, LDPE). BIONOLLE PBSu is a semicrystalline polymer that has a high crystallization ability (35-45 %) (Gigli et al. 2016). It has a melting point that is similar to LDPE and stiffness that is between LDPE and HDPE. Its glass transition temperature is  $-32^{\circ}\text{C}$ , which makes it highly workable and processable through injection molding, extrusion and thermoforming (Gigli et al. 2016). The mechanical properties of PBSu show that it is a strong and soft material that can be compared to the polymers often used in tissue engineering such as PE and PP (Ferreira et al. 2017). PBSu is a soft and strong polymer similar to LDPE, but in addition it is also biodegradable in compost, moist soil, etc. (Fujimaki 1998)

**Table 1.** *Typical properties of PBSu (grade 1000 BIONOLLE) and some polyolefins. (Fujimaki 1998)*

	PBSU (BIONOLLE #1000)		LDPE	HDPE	PP
DENSITY (G/CM <sup>3</sup> )	1.5	26	0.8	11	3
MELTING POINT (°C)	114	114	110	129	163
GLASS TRANSITION (°C)	-32	-32	-120	120	-5
YIELD STRENGTH (KG/CM <sup>2</sup> )	336	364	100	285	330
ELONGATION (%)	560	323	700	300	415
STIFFNESS 10 <sup>3</sup> (KG/CM <sup>2</sup> )	5.6	6.6	1.8	12	13.5
COMBUSTION HEAT (CAL/G)	5550		>11000		

PBSu is also biocompatible, which with its good chemical and physical properties, has made it the focus of many biomedical studies. These have been mainly concerning the production of biomaterials and drug delivery systems (Ferreira et al. 2015; Ferreira et al. 2017). It is quite hydrophobic though, which can cause some challenges in its use in tissue engineering applications since it has been shown that the surface wettability can affect the cell adhesion and proliferation. The surface chemistry, roughness and wettability are

in fact the three most important factors that affect the biological reactions on the material surface. (Arima & Iwata 2007; Carrasco et al. 2010) The cell adhesion and proliferation on PBSu scaffolds can be increased for example by modifying the scaffold surface topography and blending or copolymerizing PBSu with other more hydrophilic polymers. (Gigli et al. 2016)

### 2.1.2 Biodegradation

Polymers that are used for temporary biomedical applications need to have an appropriate biodegradation rate in physical conditions. PBSu is sensitive to enzymatic, hydrolytic and biological degradation in a reasonable time period, which is one of the reasons it has become an interesting polymer to be used in tissue engineering applications (Ferreira et al. 2017).

Aliphatic polymers like PBSu are known to degrade *in vitro* by a two-stage hydrolytic bulk degradation process (Figure 2). The first step is a random chain scission, where the molecular weight of the polymer decreases. The second step, mass loss, starts when the polymer molecular weight drops to the critical value of approximately 13 000 Da. When analysing the polymer degradation, the most extensively used techniques are measuring the weight losses as well as the changes in the molecular weight as a function of incubation time. (Gigli et al. 2016)

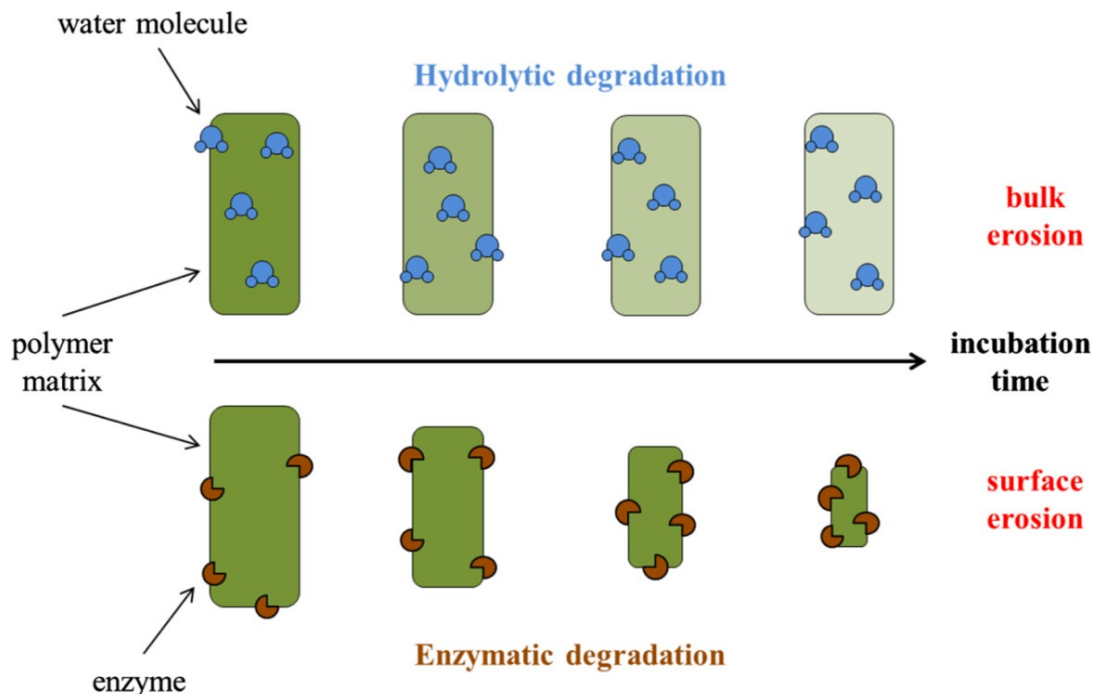


**Figure 2.** Hydrolytic and enzymatic degradation process (Gigli et al. 2016).

Many *in vitro* studies have shown that PBSu undergoes very slow hydrolytic degradation in physiological conditions. In these studies, only a decrease in the molecular weight was detected, while the polymer weight remained quite constant for several weeks. (Haiyan et al. 2005; Han et al. 2005; Gualandi et al. 2012; Almeida et al. 2013) The polymer's molecular weight, hydrophilic-hydrophobic balance, chemical structure and degree of crystallinity all affect the polymer degradation. Therefore, if needed the degradation rate can be altered by changing these polymer characteristics. (Gigli et al. 2012)

### 2.1.3 PBSu in tissue engineering

PBSu is a relatively recently developed polymer and has mainly been used for environmental purposes such as mulching films, biodegradable packaging, compostable bags as well as nonwoven sheets and textiles. This is why it has not yet been studied for bio-material applications as thoroughly as some other synthetic biodegradable polyesters like polylactide (PLA), poly( $\epsilon$ -caprolactone) (PCL) and poly(lactide-co-glycolide) (PLGA). (Brunner et al. 2011) In recent years, however, there has been a growing number of reports about the use of PBSu and PBSu-based copolymers in tissue engineering and controlled drug delivery research (Gigli et al. 2016). The *in vitro* studies have shown promising results in terms of the PBSu cytotoxicity as well as the proliferation and differentiation of human mesenchymal stem cells (hMSCs) and osteoblasts cultured on PBSu scaffolds. (Brunner et al. 2011)

One of the most studied tissue engineering fields for PBSu is bone and cartilage tissue engineering. Chitosan-PBSu scaffolds for example have been widely studied for bone repair (Oliveira et al. 2008; Alves da Silva et al. 2010; Oliveira et al. 2011). In addition, PBSu-hydroxyapatite composites (Kaewkong et al. 2012; Uppanan et al. 2013), surface hydrolysed PBSu scaffolds (Kosorn et al. 2010) as well as PBSu microspheres in carboxymethyl chitosan scaffolds (Meesap et al. 2010) have been researched for the same purpose. These studies have shown that the PBSu-based scaffolds have the ability to stimulate the osteogenic differentiation of stem cells. (Costa-Pinto et al. 2014)

PBSu-based composites have been investigated *in vitro* for bone regeneration purposes using hMSCs. The studies focused on comparing the PBSu composite films with surface modified PBSu composite films. The cell viability, adhesion and proliferation were found to be significantly better on the hydrolysed surfaces. This is explained by the hydrolyzation improving the surface roughness and therefore increasing the film hydrophilicity, which can improve osteogenesis. (Arphavasin et al. 2013; Ngamviriyavong et al. 2014)

The molecule release from PBSu-based copolymer and composite films has also been studied in order to determine their suitability for drug delivery applications (Gualandi et al. 2012). For example, films that contained fluorescein isothiocyanate (FITC) were prepared by solvent casting from PBSu and its multiblock copolymers with poly(triethylene succinate) (PTES). All of the tested materials showed a diffusion-driven FITC release

profile, with a burst release detected within the first 6 hours followed by a slower steady release. The release profiles of the different polymers varied significantly depending on their hydrophilicity and chain mobility. As the most hydrophobic material, PBSu displayed the slowest release, while the addition of the more hydrophilic PTES monomers increased the FITC release. According to Gualandi et al. (2012) the polymer crystallinity slows down the molecule release during the initial burst phase. In time however, the switch from diffusion-based release mechanism to an erosion-based release as a result of polymer hydrolysis evens out these differences caused by the crystallinity. (Gualandi et al. 2012)

## 2.2 Methods for film manufacturing

One of the main problems when studying biomaterial scaffolds *in vitro* is that the environmental cues available to the cells differ drastically from those the cells receive in their natural environment (McCarthy et al. 1996). Different techniques have been used to prepare porous and fibrous scaffolds that mimic the natural extracellular matrix (ECM) structure. These techniques include for example particulate leaching (PL), breath figure method (BF), electrospinning and phase separation (Wang et al. 2013). The first two can be prepared by solvent casting, which means that the polymer is dissolved in an organic solvent and cast onto a surface such as a petri dish. These two methods will be explained in more detail in the following sections.

### 2.2.1 Particulate leaching

In PL, water-soluble particles such as salt or sucrose are mixed with a polymer-organic solvent solution. After solution casting and solvent evaporation, a dry film is formed. The particles are then leached out of the film by washing with water, leaving behind pores where the water-soluble particles used to be (Figure 3). (Liao et al. 2002)

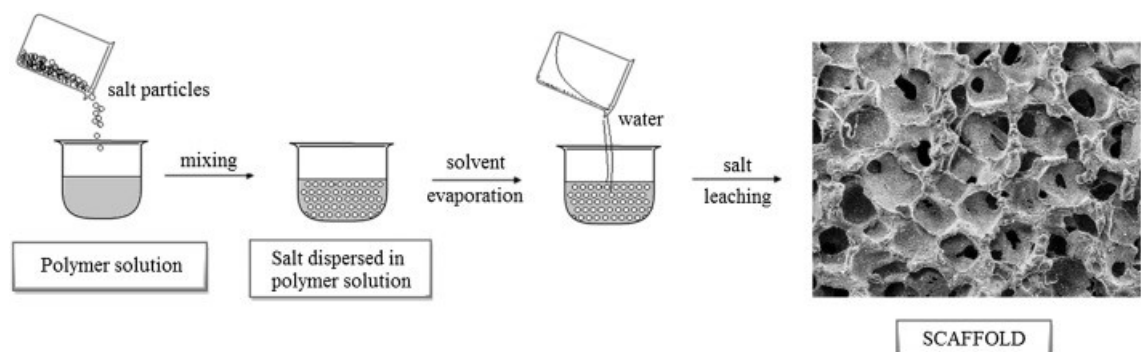


**Figure 3.** A schematic presentation of the particulate leaching method. (Janik & Marzec 2015)

The PL method is a very simple way to prepare porous scaffolds with a specific pore size and porosity by changing the particle size and amount of added porogen. (Mikos et al.

1994) The main disadvantage of the PL method is, however, that the particle distribution within the polymer solution is typically not uniform. This is due to the differences between the densities of the polymer solution and the solid particles. Another drawback of the method is that the particles can be completely wrapped by the polymer. In this case the particle is stuck inside the scaffold and it cannot be washed away with water. (Mikos et al. 1994; Hutmacher 2000)

Scaffolds prepared by PL method have been studied for various tissue engineering applications. For example, PCL scaffolds (thickness = 0.8 mm) made porous with sodium chloride (NaCl) particles ( $\phi$  400-500  $\mu\text{m}$ , polymer/NaCl = 1/30 (w/w)) and cultured with mouse fibroblasts (L929) and mouse calvaria-derived pre-osteoblastic cells (MC3T3-E1) showed promising results about their suitability for bone tissue engineering. These scaffolds had irregular pores with a pore size of  $421.27 \pm 34.18 \mu\text{m}$ . (Thadavirul et al. 2014) Also, porous sheet-like poly(L-lactide-co- $\epsilon$ -caprolactone) (PLCL) scaffolds (thickness = 150  $\mu\text{m}$ ) for soft-tissue engineering were prepared with combined particulate leaching of salt particles ( $\phi$  33-45  $\mu\text{m}$  and 45-53  $\mu\text{m}$ ) and magnetic fructose particles ( $\phi$  45-53  $\mu\text{m}$ ). The magnetic fructose particles assembled for 1-3 layers at the bottom of the scaffold and the salt particles then filled the top side with the extra PLCL solution. The porosities of these films varied between 45 % and 70 %. (Hu et al. 2013)

PBSu based PL scaffolds have been studied most widely for different bone repair applications. For example, mesoporous magnesium silicate and PBSu composite films (thickness = 2 mm) were prepared by salt leaching. Films with highly interconnected pores ( $\phi \sim 400 \mu\text{m}$ ) and porosity of 65-70 % were formed by this method. Culturing them with MC3T3-E1 showed that they promoted osteogenic differentiation *in vitro*, while implanting them into the defects of rabbit femur cavity promoted bone regeneration *in vivo*. (Wu et al. 2016) PBSu based PL scaffolds have also been studied to preserve bone mass from the residual ridge resorption in a tooth socket. NaCl powder formed pores with a diameter of 300 to 400  $\mu\text{m}$  to these scaffolds that had thicknesses of 3 mm or  $8.6 \pm 0.3 \text{ mm}$ . Culturing them *in vitro* with the MC3T3-E1 showed that also these PBSu based scaffolds were biocompatible with the osteoblast-like cells and the cells adhered well to the scaffold surface. (Hariraksapitak et al. 2008) Overall, these PBSu based scaffolds prepared by the PL method are potential candidates for bone repair applications due to their good biocompatibility, biodegradability and osteogenesis.

The studies using the PL method for tissue engineering mostly concern thick scaffolds prepared with large particles leading to formation of large pores. These differ drastically from the films that could be used for retinal tissue engineering, since for this specific application, the films should have a thickness of around 20  $\mu\text{m}$  and preferably a pore size of  $< 5 \mu\text{m}$ .

## 2.2.2 Breath figure method

The BF method is a simple, inexpensive and robust way to form honeycomb (HC) structured polymer films. This is done by solvent casting in high humidity under an airflow so that the water vapor condenses on the organic liquid surface and forms small droplets. These droplets leave pores behind on the film surface when the solvent and water have evaporated (Figure 4).

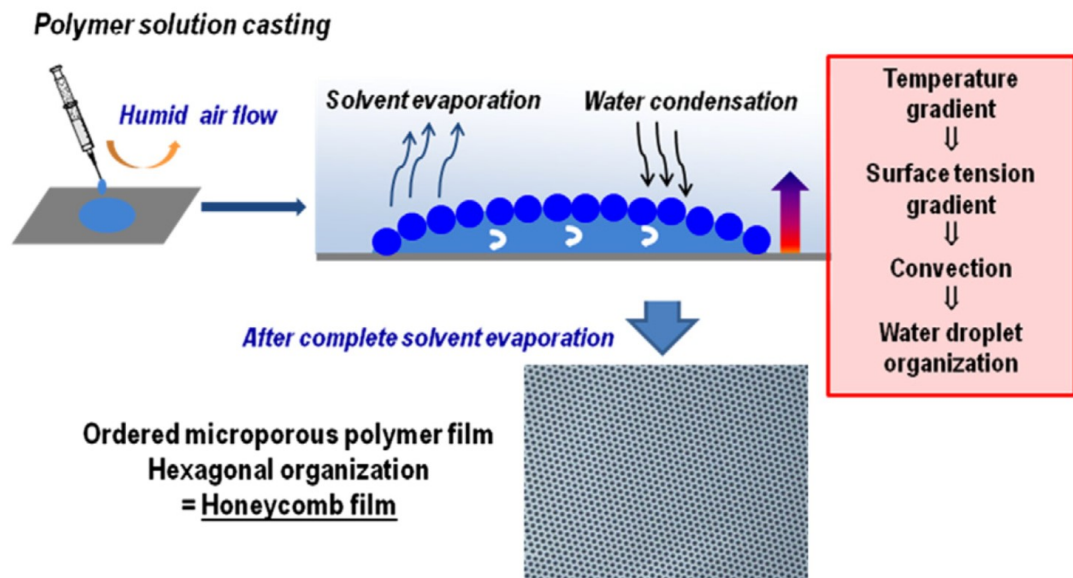


**Figure 4.** A schematic presentation of the breath figure method (Escalé et al. 2012).

There are different factors that affect the pore formation in the BF method; one of them is the choice of the solvent. The solvent should have a higher density than water, a low boiling point, a high vapor pressure, as well as low solubility in water. (Escalé et al. 2012) The pore size of the HC film can be reduced by increasing the polymer concentration because the higher concentration increases the polymer's capacity to stabilize a larger surface area of the water droplets. Also, the relative humidity plays an important role in forming HC. A humidity over 50 % is highly recommended and typically the pore regulation improves and pore size increases in higher humidity. The pore regulation is also affected by the airflow: with a lower airflow the solvent evaporates slower, which means the water droplets have more time to coalesce and therefore form fewer bigger pores. (Stenzel et al. 2006)

In the BF method, a surfactant is often used to lower the surface tension at the water-polymer solution interfaces. The surfactants are amphiphilic molecules that have a hydrophilic group as well as a long hydrophobic group. They self-assemble at the water-organic solvent interface in a way that the hydrophilic group is oriented towards the water phase and the hydrophobic end towards the solvent. This leads to lower surface tension which

reduces the coalescence of the water droplets and therefore results in smaller droplets and pores formed on the film. (Zhang & Wang 2007)

Previously it was thought that only star shaped polymers could form HC structures with BF method, but recently it has also been shown that certain linear polymers can form a solid HC structured polymer layer at the water-solvent interface. However, these polymers must have the right kind of polymer structure. The most important factor of this is that their hydrophobic chains have hydrophilic end groups. This increases the polymers segment density and therefore allows the polymers timely precipitation around the water droplets. The casting conditions also need to be carefully optimized in order for these linear polymers to form HC structures whereas the star-shaped polymers can form them in less specific conditions. (Stenzel et al. 2006)

The defined surface topography of HC films can affect the cell behaviour. The pores can mimic the native ECM microtopographical structures and therefore induce the cell adhesion, proliferation and function. Hence, HC films prepared by BF method are widely studied to be used as scaffolds for tissue engineering. (Calejo et al. 2018) For example, cardiac myocytes cultured on PLA and PCL HC films expressed good cell adhesion and function (Nishikawa et al. 2002; Arai et al. 2008). Similarly, rat cardiomyocytes and porcine aortic endothelial cells cultured on fibronectin coated PCL HC films formed strong focal adhesions (FA) over the entire cellular surface (Yamamoto et al. 2006). These HC films also promoted the ECM protein secretion (Tanaka et al. 2007). In addition, PLGA, PLA and PCL HC films have shown promising results for bone and cartilage tissue engineering using anchorage-dependent osteoblast-like MG-63 cells and rabbit articular chondrocytes respectively (Fukuhira et al. 2008; Chaudhuri et al. 2008; Eniwumide et al. 2014).

Stem cell differentiation also highly depends on the membrane surface topography. Hence, the HC structured films prepared by the BF method have attracted attention in the stem cell differentiation modulation in recent years. (Calejo et al. 2018) Also the behaviour of human embryonic stem cell-derived retinal pigment epithelium (hESC-RPE) cells have been studied on PLA HC films. The results showed that the hESC-RPE was able to adhere and proliferate on the HC structured surface in serum-free conditions and express RPE-specific markers after 6 weeks of culture. (Calejo et al. 2016; Calejo et al. 2017).

## **2.3 Retina**

The human eye is a highly organized, complex organ that has multiple different cell layers all of which have a special function. It has three main layers: the outermost layer that consists of the cornea and sclera, the vascular middle part consisting of the choroid, ciliary body and iris, and finally retina, the innermost layer. The retina is formed by the photoreceptor layer, the RPE layer and Bruch's membrane (BM) (Figure 5). It detects light and converts the energy of the absorbed photons into neural activity. (Davson 1980)

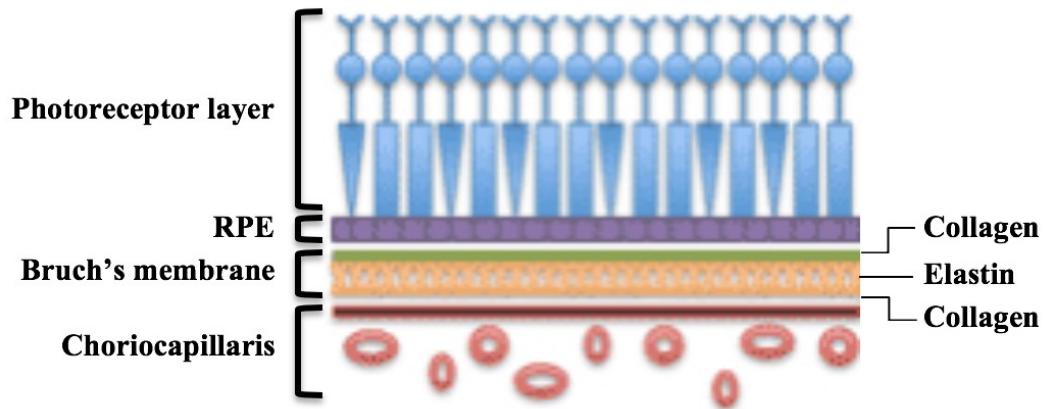


**Figure 5.** *The structure of the retina and its different layers. (Haugsdal & Sohn 2013)*

The photoreceptor layer consists of two types of photoreceptor cells: rods and cones. These differ from one another in many ways including their shape, the type of photopigment they contain, their pattern of synaptic connections and their distribution across the retina. The rod cells are very sensitive to light but have a low spatial resolution, whereas the cone cells have a high resolution in expense of their light sensitivity. The cone cells are also responsible for the detection of colours. (Purves 2009)

The choriocapillaris is a bed of highly interconnected capillaries that lie underneath the retina. The choriocapillaris's wall facing the BM is highly fenestrated, which allows the fluids and macromolecules to move into the extracapillary region and further to the basal side of the RPE through the BM. The choriocapillaris together with the BM and the RPE forms the outer blood retinal barrier (BRB). The RPE and BM structures and functions are explained in more detail in the following chapters. (Soubrane & Coscas 2013)

### 2.3.1 Retinal pigment epithelium

The RPE is a highly specialized and pigmented cell monolayer located at the interface between the photoreceptors and the BM (Figure 5). It forms the outer BRB together with the BM and the choriocapillaris. (Rizzolo 2014). RPE cells have a hexagonal cell morphology and form a tightly packed epithelium. The long apical microvilli of the RPE interact with the photoreceptor outer segments (POS), while the BM is attached to the RPE basolateral membrane. (Strauss 2005; Burke 2008; Simó et al. 2010)

### 2.3.2 Retinal pigment epithelium function

In the human eye, the light sensitive photoreceptor cells are responsible for vision. In order to maintain the light transduction capacity of the photoreceptors, the POS goes through constant renewal. The RPE plays an important role in this. The POS is phagocytosed by the RPE, where they are digested and finally the molecules are redelivered back

to the photoreceptors to be used in the POS reformation. (Simó et al. 2010; Kaarniranta et al. 2013; Rizzolo 2014) The pigments in the RPE such as melanin and lipofuscin also absorb the excessive and scattered light, which increases the optical quality of the eye. (Strauss 2005; Boulton 2014). Since the RPE forms the BRB, and the tight junctions between the RPE cells regulate the diffusion through the paracellular space in a semi-selective manner, it is also responsible for transporting water, nutrients, waste products, growth factors and metabolites between the neural retina and the choroid. (Rizzolo et al. 2011; Rizzolo 2014)

### 2.3.3 Bruch's membrane

The BM is a thin ECM structure located between the RPE and the choriocapillaris (Figure 5, Figure 6). Its thickness is around 2-4  $\mu\text{m}$  and it is composed of five different layers: the basement membrane of the RPE, the inner collagenous layer, the elastin layer, the outer collagenous layer and the basement membrane of the choroid. (Sumita 1961; Booij et al. 2010) The outermost layer, the basement layer of the RPE, is mainly formed of collagen IV, laminin and fibronectin and it forms a good base for the RPE cells to attach. (Booij et al. 2010) The BM has good mechanical properties most likely due to the presence of collagen and elastin in high concentrations. (Skeie 2010) The schematic illustration of the BM structure and its main components is presented in Figure 6.

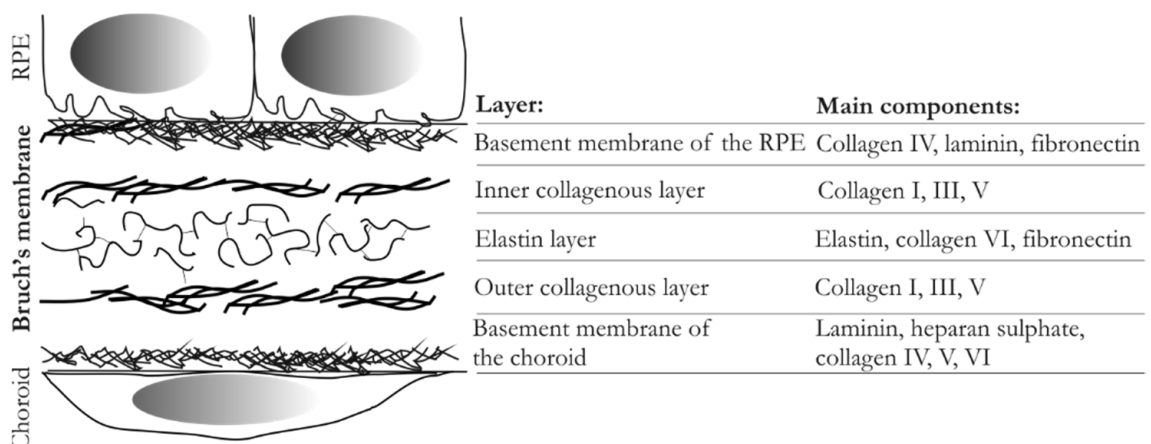


**Figure 6.** The structure and main components of the human Bruch's membrane layers (Sorkio 2016).

The BM has many different functions in the retina. First of all, it provides structural support and a favourable base for the RPE cells to attach, migrate and differentiate (Gong et al. 2008). As mentioned earlier, it also forms the BRB with the RPE by acting as a semi-permeable membrane for the oxygen, nutrient, metabolic waste, fluid and biomolecule exchange between the retina and the choriocapillaris. The BM also prevents the cell migration between the retina and the choroid. (Booij et al. 2010)

During ageing, function of the BM can be altered due to membrane thickening, reduced filtration capacity, calcification of elastic fibers and an increased collagen fiber crosslinking (Ramrattan et al. 1994; Curcio & Johnson 2013). All of these changes can play a part in the development of age-related macular degeneration (AMD) through neovascularization or complement activation. (Booij et al. 2010) In patients with AMD, the BM no longer supports the cell attachment and other normal functions of the RPE, which results in the degeneration of the adjacent RPE cells and photoreceptors. (Del Priore et al. 2006)

### **2.3.4 Age-related macular degeneration**

Because of the highly important roles of the RPE, the failure of one or more of these can easily lead to retinal degeneration and vision loss. Thus, AMD is the leading cause of central blindness in developed countries and is expected to affect almost 200 million people worldwide by 2020 (Wong et al. 2014).

There are two types of AMD: wet (neovascular) and dry (atrophic). Wet AMD (the most severe form of AMD) is caused by the choroidal capillaries growing into BM and RPE (Feeny et al. 2015). This excessively growing choroidal neovascularization exudes blood, fluid and lipids to the neural retina and causes fibrous scarring and acute vision loss (Bonilha 2008). Dry form AMD, on the other hand, is caused by progressive atrophy of the RPE, choriocapillaris as well as the neighbouring photoreceptors. (Ambati & Fowler 2012; Lim et al. 2012) Both AMD phenotypes are caused by the combination of changes in the structure of the BM, degeneration of the RPE as well as drusen formation that leads to photoreceptor dysfunction and, in time, loss of vision. (Lim et al. 2012) The treatment options that are currently available work on delaying the progression of wet AMD only, so there is a pressing need for effective treatments for dry AMD (Ambati & Fowler 2012; Riera et al. 2016). Cell therapies involving pluripotent stem cell (PSC)-derived RPE cells have shown the most promise in reversing the degeneration and vision loss and have therefore become the main focus in the study of regenerative medicine for AMD. (Kaarniranta et al. 2013)

### **2.3.5 Human embryonic stem cell-derived RPE**

hESCs are derived from the inner cell mass of preimplantation embryos and can be indefinitely expanded *in vitro*. hESCs can also differentiate to mature cell types of any germ layer, including RPE. (Thomson et al. 1998) There are two approaches to the hESC differentiation into RPE: spontaneous differentiation and directed differentiation. The spontaneous differentiation can be induced by changing some of the molecular cues like removing the basic fibroblast growth factor (bFGF) that keeps hESCs pluripotent *in vitro*. When the bFGF is removed, the hESCs start to differentiate and pigmented areas of RPE cells can be manually picked from the cultures to be cultured further in order to get a pure population of RPE cells. Even though spontaneous differentiation works, it is not very

effective since it takes several weeks of culture to get enough hESC-RPE cells (Vaajasaari et al. 2011). The directed differentiation, on the other hand, uses the natural signalling methods used for the RPE development *in vivo*. In the first step, factors such as dickkopf-related protein 1, nicotinamide, Lefty-A, N2 and B27 are used to guide the hESC differentiation towards neuroectoderm. In the second step, a fibroblast growth factor inhibitor SU5402 and Activin-A are used to direct the differentiation towards RPE rather than neural retina. (Vaajasaari et al. 2011; Buchholz et al. 2013) In addition to being faster, Leach et al. have recently shown that the directed differentiation is also a more reliable method for producing hESC-RPE than the spontaneous differentiation. (Leach et al. 2016)

hESC-RPE is a mature and functional RPE with morphological similarities to the native RPE such as having polygonal, cuboidal epithelial cell morphology and high rate of pigmentation. (Garcia et al. 2015; Hongisto et al. 2017) In addition to the consistent structure of a mature RPE that the hESC-RPE shows, it also displays the ability to phagocytose the POS and secrete growth factors. (Hongisto et al. 2017) Furthermore, the hESC-RPE injected into animal models also improved the functional performance of the RPE when compared to the controls. (Stern & Temple 2011)

These results together with the hESC's high self-renewal capacity make hESC-RPE cells potential candidates for retinal cell therapies. Clinical trials transplanting hESC-RPE cell suspension to human patients with AMD and Stargardt's Macular Dystrophy also confirmed the safety of hESC-RPE transplantation. There was no tumour formation, hyperproliferation or other major complications observed during the 22-month follow-up. In addition, the results showed RPE thickening, which indicates that the transplanted cells integrated successfully to host RPE. Some improvement in patients' visual acuity was also detected. (Schwartz et al. 2016)

### **2.3.6 Cell adhesion**

Integrins are heterodimers that mediate the interactions between the ECM molecules and cells by participating in cell adhesion, migration, differentiation, cell survival and other cellular functions (Figure 7). RPE cells express various integrin sub-units that can bind to extracellular ligands from the BM such as laminin, collagen and fibronectin in order to promote RPE cell adhesion. Different methods of manipulating integrins have been studied for improving cell survival post-transplantation (Afshari & Fawcett 2009), but it has also been shown that a longer cell culture period before transplantation increases the integrin expression on the cell surface and therefore improves the cell adhesion. (Gullapalli et al. 2008)

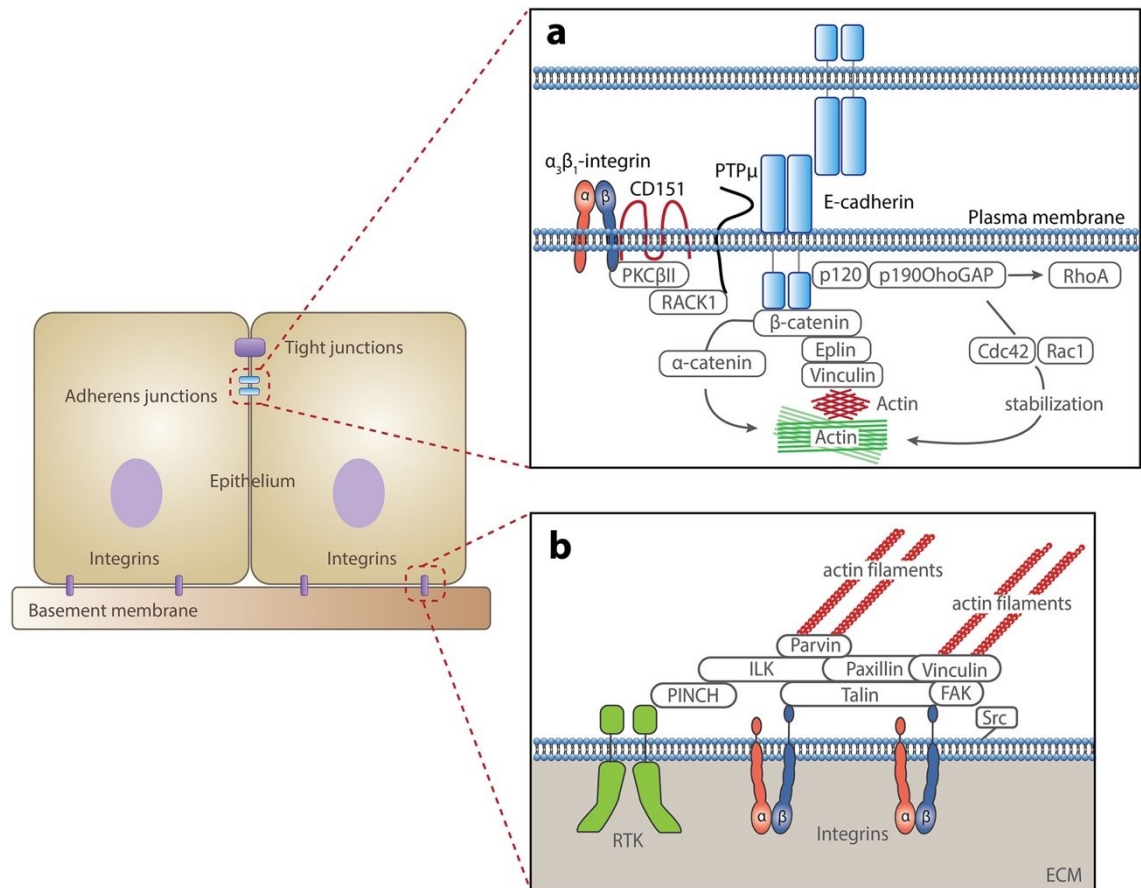


**Figure 7.** A scheme showing (a) the cell–cell junction and (b) the cell–matrix junction and how vinculin plays a part in those (Goldmann 2016).

Vinculin is an amphitropic protein that exists in the cell as a soluble cytoplasmic as well as a membrane bound protein. Vinculin has been reported to bind for example talin and F-actin. At focal adhesions (FAs) integrins connect the actin cytoskeleton to the ECM. When mechanical forces are present, vinculin becomes active and helps strengthen the FAs by crosslinking the F-actin to the talin molecule (Figure 7b). (Golji et al. 2011) It has been shown that in addition to the FA formation, vinculin also controls the cell migration. Therefore, loss of vinculin can lead to problems with cell migration and cell adhesion, both of which are critical processes for tissue growth. (Goldmann 2016)

A common problem with the RPE transplantations has been the limited functional recovery of the transplanted RPE, particularly when the cells are administered in suspension. This is due to fact that RPE cells are anchorage-dependent, thereby dying soon after the transplantation, and due to their limited migration out of the site of implantation. (Tezel & Del Priore 1997) When using synthetic biomaterials as cell carriers, biofunctionalization such as physical or chemical modification is usually needed to improve the cell attachment to the surface. Physical modification includes coating the material with proteins like collagen and laminin. (Calejo et al. 2018) This coating can be done by absorption or Langmuir-Schaefer film deposition (Sorkio et al. 2015; Calejo et al. 2017). Alternatively, creating new functional groups on the polymer surface by plasmatreatment with reactive

gases is a commonly used chemical modification technique (Tallawi et al. 2015). The cell adhesion, morphology, alignment and cellular functions can also be improved by modifying the microscale biomaterial surface topography, e.g. size, geometric arrangement and shape of surface features (Nguyen et al. 2016).

## 3. MATERIALS AND METHODS

The polymer used in this study was BIONOLLE 1020MD (LOT NJ226BP11, 5.12.2012). The reference films used in cell culture were commercial polyethylene terephthalate (PET) Millicell cell culture inserts with 1  $\mu\text{m}$  pore size (film size = 0.3  $\text{cm}^2$ , Millipore). For cell culture a hESC line Regea 08/017 was used. These hESCs had been differentiated into RPE cells as described by Hongisto et al. (Hongisto et al. 2017)

### 3.1 Film preparation

The study was started by manufacturing PBSu films by solvent casting. The solvent used for this was chloroform. Later on, the films were made porous by using particulate leaching as well as breath figure method.

#### 3.1.1 Solvent casting

The films were prepared by solvent casting, where the polymer pellets were dissolved in chloroform while stirred with a magnetic stirrer. This solution was then cast on glass Petri dishes with a diameter of 40 mm (Steriplan®) and the chloroform was allowed to evaporate overnight in a fume hood at room temperature. Before making the films porous, solid PBSu films were prepared with different polymer concentrations and casting volumes (Table 2) inside a fume hood in humidity of ~40 %. This was done in order to identify the optimal conditions leading to the production of films with appropriate thicknesses for this application.

**Table 2.** *The concentrations and casting volumes studied before adding any porogens.*

CONCENTRATION (% W/V)	CASTING VOLUME (ML)
0.3	0.5
0.3	1.0
0.5	0.5
0.5	1.0
0.8	0.5
0.8	1.0
1.0	0.5
1.0	1.0
1.5	0.5
1.5	1.0
2.0	0.5
2.0	1.0
3.0	0.5
3.0	1.0
5.0	0.5
5.0	1.0

### 3.1.2 Particulate leaching

For this study, sucrose microparticles were chosen to be used as a porogen. The particle sizes were determined by measuring the particles from an optical microscope (Olympus, BH-2, GWB) image taken with a digital camera (BUC4-500C, BestScope) attached to the microscope. An optical microscope image of the sucrose particles is presented in Figure 8, where it can be seen that the particle size varied between 1  $\mu\text{m}$  and 3  $\mu\text{m}$ . This is quite optimal for RPE cell culture since the pore size for them should be around 5  $\mu\text{m}$ . Pores within this size range enable diffusion of small molecules and ions, but at the same time are small enough to prevent the RPE cell migration across the material. (Calejo et al. 2016)

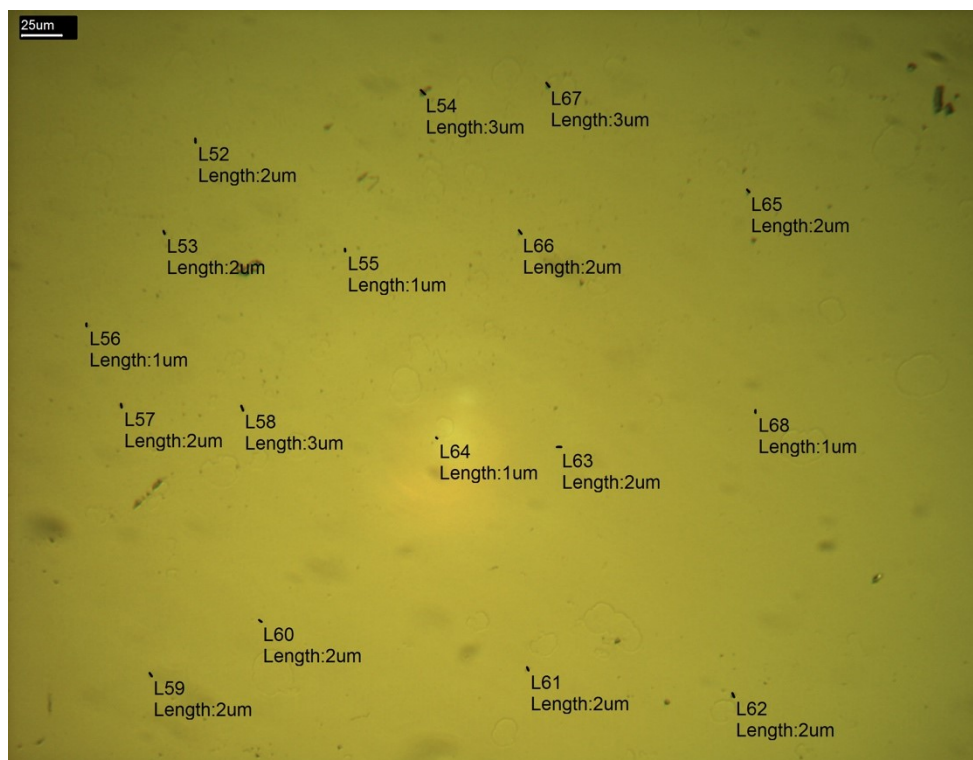


**Figure 8.** *An optical microscopy image with 20 $\times$  magnification showing the size distribution of the sucrose particles.*

Sucrose particles were nonetheless found to aggregate to some extent. To minimize the presence of these aggregates, two solutions were prepared; one with PBSu dissolved in chloroform and one with sucrose particles and chloroform. The sucrose solution was placed in an ultrasound bath for 30 minutes and then stirred with a magnetic stirrer for another 30 minutes. These steps were also repeated once more. After the sonication and mixing cycles, the sucrose solution was left to stand for 60 minutes so the biggest aggregates still present in the solution would sink to the bottom of the vial. The supernatant of the sucrose solution was then mixed with the polymer solution to form a solution that had a specific polymer and sucrose concentration. This solution was once more left to stand for 60 minutes so possible aggregates would sink and not end up in the films.

Careful not to mix the solution, the supernatant was cast inside a fume hood the same way as described previously in chapter 3.1.1, but this time the humidity varied between 30-55 %. After the solvent was evaporated, the films were rinsed with distilled water. After that, they were left to soak in 4 ml of distilled water for 24 h so the sucrose particles would wash off. The water was changed several times during this step. After this was completed, the films were left to dry in the fume hood overnight and were then placed in a vacuum chamber in order to remove the residual water. Samples were left in the vacuum chamber until further analysis. Different sucrose concentrations (5-25 %) were tested, where the sucrose amount was calculated as a weight % relative to the PBSu weight used in the study. The PBSu concentrations, casting volumes and sucrose concentrations used are indicated in Table 5.

### 3.1.3 Breath figure method

PBSu solutions were initially prepared in chloroform. The polymer was let to dissolve overnight at room temperature under constant stirring. 1,2-dioleoyl-sn-glycero-3-phosphoethanolamine (DOPE, Sigma, Japan), used as a surfactant in the BF method, was dissolved in chloroform. The DOPE solution was then mixed with a PBSu-chloroform solution to form a solution with the desired polymer and DOPE concentrations. This mixture was let to rest for an hour before being cast on a similar petri dish as used before (3.1.1, 3.1.2) and quickly placed in a chamber (Figure 9) under humid air flow (relative humidity, RH % =  $82 \pm 3$  %). After chloroform had evaporated, the film was placed inside a fume hood overnight to make sure there were no chloroform residues, and to allow evaporation of the condensed water droplets. The films were then rinsed three times with distilled water in order to extract all the surfactant from the films. After drying inside the fume hood, they were moved to a vacuum chamber to remove any residual water and to wait for further analysis. Different DOPE concentrations were tested, and the DOPE amount was calculated as a weight-% relative to the PBSu weight used in the study.

Different PBSu and DOPE concentrations and casting volumes were tested in order to get homogeneous films with a HC surface structure and appropriate thickness. As mentioned earlier, the optimal pore diameter for RPE cell culture is around 4-5  $\mu\text{m}$  so the goal was to prepare films with this pore size.

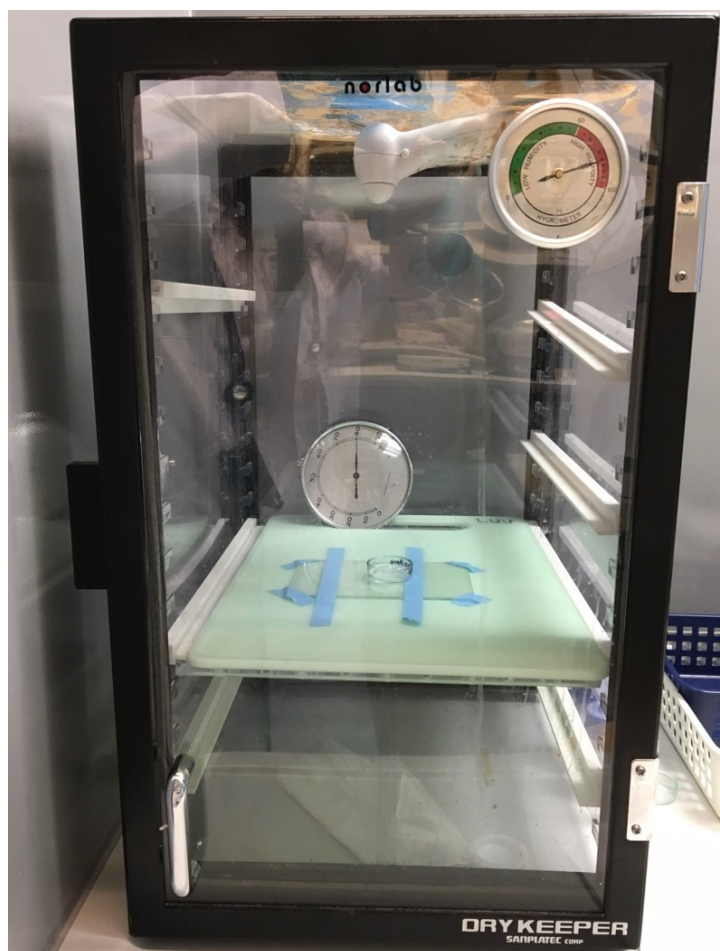


**Figure 9.** *The humidity chamber used for preparation of PBSu films by the BF method. Inside the chamber, a fan placed above the sample ensured the fast evaporation of the solvent.*

## 3.2 Film characterization

### 3.2.1 Macroscopic and microscopic features

The homogeneity of the films and the evenness of the polymer distribution were first checked visually. The optical microscope with a 20× objective was then used to observe the film surface in more detail. Images of each of the films were taken with this microscope and they were used to measure the diameters of possible pores present on the film surface.

The sample surface topography was analysed by imaging with an atomic force microscope (AFM, XE-100, Park Systems Corp, USA) according to the device instructions. An area of 40 μm × 40 μm was scanned in noncontact mode. The imaging was done under air at room temperature with an APPNANO AFM cantilever (type ACTA, L = 125 μm, tip radius < 10 nm, f = 200-400 kHz, spring constant = 25-75 Nm<sup>-1</sup>, coating aluminium).

The images were edited and analysed with XEI image processing software (Park Systems). The pore sizes were determined from these images as well as the arithmetic mean of surface roughness ( $R_a$ ) values.

### **3.2.2 Determination of film thickness**

The thicknesses of the dry films were measured with a micrometer (Mitutoyo). Three different areas of each film were measured.

### **3.2.3 Water contact angle**

The film surface wettability (hydrophilicity) was measured with a water contact angle (WCA) measurement. Measurements were carried out by the sessile drop method using a Theta Lite optical densitometer (Attension, Biolin Scientific AB, Sweden) at room temperature. A drop of water was placed on the surface of the film and images of the droplet were taken at time points of 0 s (as soon as the drop was placed), 6 s and 12 s. From those images the right and left side angles of the drops were measured. Two replicates of each film were used and the WCA measurements were done twice for each sample. The first measurements for the BF method films were done without washing away the surfactant. However, since the presence of the surfactant could affect the results, these measurements were repeated with films that were washed with distilled water.

### **3.2.4 Electrical resistance**

The electrical resistance through the films was measured. The films were initially rinsed with 70 % ethanol and soaked in Dulbecco's phosphate-buffered saline (DPBS) for 10 min before being clamped between P2307 sliders (Physiologic Instruments, USA) and assembled to a custom-made Teflon chamber. For the measurement, the sliders were submerged in DPBS and the electrical resistance was determined by using a Millicell electrical resistance system volt-ohm meter (Merck Millipore, Germany). Four independent films per sample type were analysed, and two measurements were done per film.

### **3.2.5 *In vitro* stability of PBSu films**

Hydrolysis series was done for the PL films of 1 % and 2 % PBSu with 5 % sucrose, their control films without any sucrose, as well as the BF films of 2 % PBSu with 5 % DOPE and its control films without any surfactant. The series had four different time points: 2 weeks, 4 weeks, 8 weeks and 16 weeks. Three replicates of each film were used for each timepoint. The series was done by placing a small, pre-weighed, piece of film (approximately 1 cm × 1 cm) in a plastic tube with 4 ml of 0.05 M TRIS-buffer (pH 7.40 at 37 °C). These tubes were then incubated in 37 °C for 2-16 weeks while the buffer was changed every week. At each time point the three replicates of each of the films were washed with

distilled water and their wet weights measured. This was done by drying the film surface with a paper towel after which the films were weighed twice. The films were then placed in a vacuum chamber to dry completely before their dry weights were weighed twice to see if there was any mass loss detected.

From these weights, the films' relative masses and water absorptions were calculated as follows:

$$\text{relative mass} = \frac{m_f}{m_0} \times 100 \%, \quad (1)$$

$$\text{water absorption} = \frac{m_{f,wet} - m_f}{m_f} \times 100 \%, \quad (2)$$

where  $m_0$  is the initial mass of the film,  $m_f$  is the final dry mass of the film and  $m_{f,wet}$  is the final wet mass of the film.

### 3.3 Cell culture

The 2 % PBSu membranes prepared by the PL method with 5 % sucrose (2 % PBSu PL), and by the BF method with 5 % surfactant (2 % PBSu BF) were cut to  $\sim 7 \text{ mm} \times 7 \text{ mm}$  pieces. Eight pieces of each type of film were used as well as four commercial PET-membranes that were used as control films.

#### 3.3.1 Disinfecting the membranes

Inside a laminar chamber, the membrane pieces were carefully placed inside the wells of a 48-well plate (well size  $1.1 \text{ cm}^2$ ), so that their porous side was placed upwards. Inserts were then placed inside the wells on top of the membranes to prevent them from curling up and to keep them from floating. UV-light in the laminar chamber was turned on for 20 minutes while the membranes and all the equipment and reagents needed were inside. After sterilization, 500  $\mu\text{l}$  of 70 % ethanol was added inside each well in order to make sure the membranes were thoroughly disinfected. After 10 minutes the ethanol was carefully removed from the well and the membranes were washed three times with 500  $\mu\text{l}$  of sterile DPBS.

#### 3.3.2 Coating the membranes

Four PL membranes and four BF membranes as well as two commercial PET-membranes were dip-coated with a collagen-laminin solution prepared in phosphate-buffered saline (PBS) containing  $\text{CaCl}_2$  and  $\text{MgCl}_2$ . Each well was coated with 10  $\mu\text{g}$  collagen IV/ $\text{cm}^2$  and 0.75  $\mu\text{g}$  laminin 521/ $\text{cm}^2$ . Stock solutions of 1 mg/ml collagen IV and 0.1 mg/ml laminin 521 were used. PET membranes, used as controls, were dip-coated using the same protein concentrations.

Films which were not dip-coated were simply incubated with PBS containing  $\text{CaCl}_2$  and  $\text{MgCl}_2$ . Parafilm was then tightly wrapped around the plates and they were placed in a fridge (4 °C) overnight.

Later, two extra samples of each type of PBSu membrane and one PET membrane were coated with collagen and laminin in the same way as described above so they could be studied without culturing any cells on them.

### 3.3.3 Culturing the cells

After dip-coating the samples overnight, the protein solution and the PBS were removed from the wells. Membranes were washed twice with 300  $\mu\text{l}$  DPBS and twice with 300  $\mu\text{l}$  DM-medium.

A cell suspension was prepared in DM- medium. A volume of 500  $\mu\text{l}$  of the cell suspension was added to each well containing the PBSu samples. Cells were seeded at a density of 180 000 cells/ $\text{cm}^2$ .

For the PET membranes, 300  $\mu\text{l}$  of a slightly less concentrated cell suspension was added to the inner compartment of the inserts, so as to achieve the same density of seeded cells (i.e. 180 000 cells/ $\text{cm}^2$ ). 700  $\mu\text{l}$  of the DM-medium was added around the insert, inside the well.

The plates were then placed in an incubator (37 °C) for 1-5 days. The medium was changed on days 1 and 2.

### 3.3.4 Cell viability

The cell viability was assessed at time points of 1, 2 and 5 days using PrestoBlue™ (Invitrogen A13262 lot:1824890) reagent. At each time point, the cell culture medium was removed from each well and replaced with the reagent diluted with culture medium in a 1:10 (v/v) ratio. The cells were then incubated for 30 min at 37 °C with this medium mixture, after which volumes of 100  $\mu\text{l}$  aliquots of this PrestoBlue™ medium (two replicates per well) were sampled from each well on a 96-well plate. The remaining PrestoBlue™ medium solution on the cells was replaced with fresh medium and the cells were placed back to the incubator. Plain medium-PrestoBlue™ mixture without cell incubation was used as a control. The fluorescence was analysed in a 96-well plate using the Wallace Victor2™ 1420 Multilabel counter (Perkin Elmer Wallace, Norton, OH). Wavelengths of 544 nm for excitation and 615 nm for emission were used. The absorbance of the control sample was subtracted from the sample results so the absorbance of the original medium-PrestoBlue™ mixture would not affect the results.

### 3.3.5 Immunostainings

The protein expression and localization were studied with immunofluorescence (IF) staining after 1 and 5 days. Table 3 shows all the primary and secondary antibodies used for this study. Phalloidin-tetramethylrhodamine B isothiocyanate (Phalloidin, Sigma-Aldrich) was used to stain the actin cytoskeleton.

**Table 3.** *The primary and secondary antibodies used for immunostainings.*

	PROTEIN/ ANTIBODY	SUP- PLIER	SOURCE	DILLU- TION	SOLU- TION	
PRIMARY	Vinculin	V4139- 200UL	Sigma	Rabbit	1:200	1
	Collagen IV	MAB3326	Millipore	Mouse	1:200	2
	Laminin	ab11575	Abcam	Rabbit	1:100	2
	Fibron- ectin	ab23750	Abcam	Rabbit	1:500	3
SECOND- ARY	Anti- mouse A568	A21043	Thermo- Fisher	Goat	1:800	2 & ctrl
	Anti- rabbit A488	A-21206	Thermo- Fisher	Donkey	1:800	1, 2, 3 & ctrl
	Phalloidin-tetramethylrhodamine B isothiocyanate				1:300	1

To start the staining procedure, the films were washed three times with PBS for 5 minutes each. The cells were then fixed with 4 % paraformaldehyde for 10 minutes and washed again with PBS (3 × 5 min). Permeabilization of the cells was done by placing 300 µl 0.1 % Triton X-100-PBS solution into each well for 10 minutes and background interference was minimized by blocking with 3 % bovine serum albumin protein (BSA)-PBS solution for 1 hour in room temperature. After washing with PBS (3 × 5 min), the films were cut into three pieces except one of each type of the coated films in 4 pieces. These extra pieces of the coated films were left without any primary antibodies to see if there would be any autofluorescence detected that should be taken into consideration (controls).

All primary antibodies were diluted in 0.5 % BSA-PBS according to Table 3. Solution 1 and 3 contained anti-vinculin and anti-fibronectin, respectively. The primary antibodies with affinity for collagen IV and laminin were both mixed in the same solution while the primary antibodies staining vinculin and fibronectin were mixed in solution 2. 200 µl of

these primary antibody solutions (1, 2 and 3) were added on the film pieces in the wells so that there were two replicates of the PBSu films for each staining while there was only one piece of the PET films for each (Table 4). 200  $\mu$ l 0.5 % BSA-PBS was added to the wells containing the control films. The well plate was then wrapped in parafilm and aluminium foil and placed in a fridge (+4 °C) overnight.

**Table 4.** *The plan for the antibody staining showing which samples and antibody mixtures are in which wells of the well plate. 1=vinculin, 2=collagen IV and laminin, 3=fibronectin.*

		1	2	3	4	5	6	7
UNCOATED PL	A	1	1	2	2	3	3	
UNCOATED BF	B	1	1	2	2	3	3	
COATED PL	C	1	1	2	2	3	3	ctrl
COATED BF	D	1	1	2	2	3	3	ctrl
UNCOATED PET	E	1		2		3		
COATED PET	F	1		2		3		ctrl

The next day, the primary antibody solutions were removed from the wells and the film pieces were washed with PBS (3  $\times$  5 min). The secondary antibodies were diluted in 0.5 % BSA-PBS according to Table 3. For the vinculin-stained films, the anti-rabbit (A488) antibody was mixed with phalloidin, which stained the actin filaments of the cells. Both secondary antibodies were mixed together in the same solution to be used on the collagen IV and laminin stained films as well as on the control films. The anti-rabbit (A488) antibody was diluted and used on films stained for fibronectin. 200  $\mu$ l of these secondary antibody solutions were added on the film pieces and left to incubate for 1 hour in room temperature. The films were then washed with PBS (3  $\times$  5 min) before transferring them onto cover slips. When the film was on the coverslip, the excess liquid was dried and a drop of Vectashield mounting medium (Vector Laboratories, USA) was added. Vectashield included 4',6'-diamidino-2-phenylidole (DAPI) for nuclei staining. Another coverslip was immediately placed on the sample and they were sealed with nail polish. These samples were then stored in the freezer (-20 °C) until imaging with a confocal microscope.

### **3.4 Confocal microscopy**

After the cell cultured films were stained, Z-stack images of them were taken with an LSM 780 confocal microscope (Carl Zeiss). A 63× oil immersion objective lens and an image size of 135  $\mu\text{m}$   $\times$  135  $\mu\text{m}$  was used for imaging. The images were taken in order to see the cell count, cell distribution and protein formation in different types of films and to establish differences between samples. The images were edited using ZEN Black lite software (Carl Zeiss).

## 4. RESULTS AND DISCUSSION

The PBSu films were studied to act as BM substitutes. Ideally, properties of the films should be as similar to the natural BM as possible, and they should also stimulate the cell adhesion and proliferation.

### 4.1 Film characterization

This chapter focuses on analysing the film characteristics such as film thickness, film surface porosity, pore size, possible honeycomb structure and pore distribution to see if they have an effect on the film degradation, wettability or electrical resistance. Analysis methods used were optical and atomic force microscope imaging, as well as thickness, WCA and electrical resistance determination. The film degradation during the hydrolysis series was studied by measuring the water absorption of the film, mass loss and analysing the AFM images to see the possible changes in the surface structure and roughness.

#### 4.1.1 Film thickness

The natural BM is 2-4  $\mu\text{m}$  thick (Sumita 1961) so ideally the scaffold should be of similar thickness. However, polymer films this thin would be quite difficult to handle and implant surgically. On the other hand, films that are too thick could affect the diffusion of fluids, small molecules and ions through the membrane and therefore reduce the cell viability. This is why the goal was to prepare films with thicknesses around 20  $\mu\text{m}$ . Films with different PBSu concentrations, casting volumes and sucrose and DOPE concentrations were prepared. The casting conditions and film thicknesses are listed in Table 5 and Table 6.

Determination of the film thickness was critical for the optimization of film preparation. When the films revealed to be too thick or too thin, the polymer concentration and casting volume were modified accordingly. The film thickness also gives essential information about the film homogeneity.

The first five samples listed in Table 5 (PL1-5) were so thin that they could not be detached from the petri dish and therefore their thicknesses are unknown. The films with 1-3 % (w/v) PBSu were found to be the right thickness with casting volumes of 0.5, 1 or 2 ml depending on the concentration (PL6-9, 11, 13). The addition of sucrose made the films slightly thicker than they were before, which led to the 3 % PBSu films to be too thick for this application (PL23-24).

From these PL film results, 1 % PBSu with 2 ml casting volume and 2 % PBSu with 0.5 ml casting volume were chosen to be studied further, since they were the right thickness and these results were reproducible between replicates. The PL method films with and without 5 % sucrose were prepared with both of these concentrations (1 % PBSu PL, 1 % PBSu PL ctrl, 2 % PBSu PL, 2 % PBSu PL ctrl). First, the polymer, sucrose and chloroform were mixed, and this mixture was sonicated. Unfortunately, this made the films brittle and non-homogeneous which suggests that the sonication affects the polymer structure and properties. Therefore, only the sucrose and chloroform were placed in the ultrasound bath and the PBSu-chloroform solution was mixed afterwards. This resulted in more homogeneous and strong films.

For the BF method (Table 6), 1 % PBSu and 2 % PBSu with casting volumes of 0.5 ml to 2 ml were tested with various DOPE concentrations. The 1 % PBSu films were found to be less homogeneous than the 2 % PBSu films and the larger casting volumes (BF2, 4, 6, 8, 10, 12, 13, 14, 16) led to films that were too thick for retinal tissue engineering applications. Furthermore, samples prepared using 2 % PBSu in the presence of 5 % DOPE were found to have a HC-like surface structure, but only when the casting volume was 0.5 ml (BF11, 23-24, 27-43). Samples prepared in this way by the BF method (2 % PBSu BF) were investigated in further studies. For comparison, controls prepared in the absence of surfactant (2 % PBSu BF ctrl) were similarly investigated.

**Table 5.** *Thickness, and microscopic and macroscopic features of different types of PBSu PL films. +++=Very homogeneous, +=moderately homogeneous, -=moderately heterogeneous, --=Very heterogeneous.*

SAMPLE CODE	CONCENTRATION (% W/V)	VOLUME (ML)	SUCROSE CONCENTRATION (% W/W)	ULTRASOUND (MIN)	THICKNESS ( $\mu\text{M}$ )	HOMOGENEITY	OPTICAL MICROSCOPE
PL1	0.3	0.5	0	-	-	-	-
PL2	0.3	1.0	0	-	-	--	--
PL3	0.5	0.5	0	-	-	+	+
PL4	0.5	1.0	0	-	-	--	--
PL5	0.8	0.5	0	-	-	+	+
PL6	0.8	1.0	0	-	0.019 $\pm$ 0.005	--	--
PL7	1.0	0.5	0	-	0.017 $\pm$ 0.001	+	+
PL8	1.0	1.0	0	-	0.020 $\pm$ 0.004	--	--
PL9	1.5	0.5	0	-	0.022 $\pm$ 0.006	++	++
PL10	1.5	1.0	0	-	0.042 $\pm$ 0.024	--	--
PL11	2.0	0.5	0	-	0.015 $\pm$ 0.005	++	+
PL12	2.0	1.0	0	-	0.036 $\pm$ 0.006	-	-
PL13	3.0	0.5	0	-	0.023 $\pm$ 0.009	++	+
PL14	3.0	1.0	0	-	0.059 $\pm$ 0.013	-	-
PL15	5.0	0.5	0	-	0.038 $\pm$ 0.015	+	+
PL16	5.0	1.0	0	-	0.140 $\pm$ 0.033	--	--
PL17	2.0	0.5	25	-	0.033 $\pm$ 0.012	--	--
PL18	2.0	1.0	25	-	0.035 $\pm$ 0.006	--	--
PL19	3.0	0.5	25	-	0.037 $\pm$ 0.019	--	--
PL20	3.0	1.0	25	-	0.043 $\pm$ 0.022	--	--
PL21	2.0	0.5	10	2 $\times$ 15*	0.014 $\pm$ 0.012	-	-
PL22	2.0	1.0	10	2 $\times$ 15*	0.030 $\pm$ 0.006	-	-
PL23	3.0	0.5	10	2 $\times$ 15*	0.024 $\pm$ 0.006	-	-
PL24	3.0	1.0	10	2 $\times$ 15*	0.066 $\pm$ 0.068	--	-
PL25	1.0	1.5	5	2 $\times$ 25*	0.036 $\pm$ 0.013	--	--
PL26	1.0	1.5	5	2 $\times$ 25*	0.020 $\pm$ 0.007	-	--
PL27	1.0	1.5	5	2 $\times$ 25*	0.028 $\pm$ 0.009	-	-
PL28	1.0	2	5	2 $\times$ 25*	0.028 $\pm$ 0.010	--	--
PL29	1.0	2	5	2 $\times$ 25*	0.024 $\pm$ 0.012	--	--
PL30	1.0	2	5	2 $\times$ 25*	0.053 $\pm$ 0.021	-	-
PL31	2.0	0.5	5	2 $\times$ 25*	0.039 $\pm$ 0.017	--	--
PL32	2.0	0.5	5	2 $\times$ 25*	0.016 $\pm$ 0.004	--	-
PL33	2.0	0.5	5	2 $\times$ 25*	0.015 $\pm$ 0.003	-	-
PL34	2.0	1.0	5	2 $\times$ 25*	0.020 $\pm$ 0.006	--	--
PL35	2.0	1.0	5	2 $\times$ 25*	0.026 $\pm$ 0.014	-	-
PL36	2.0	1.0	5	2 $\times$ 25*	0.032 $\pm$ 0.007	-	-
PL37	1.0	1.5	5	2 $\times$ 30	0.023 $\pm$ 0.009	+	+
PL38	1.0	1.5	5	2 $\times$ 30	0.032 $\pm$ 0.029	--	-
PL39	1.0	2.0	5	2 $\times$ 30	0.018 $\pm$ 0.004	+	+
PL40	1.0	2.0	5	2 $\times$ 30	0.023 $\pm$ 0.015	-	-
PL41	1.0	2.0	5	2 $\times$ 30	0.022 $\pm$ 0.004	+	-
PL42	1.0	2.0	5	2 $\times$ 30	0.020 $\pm$ 0.014	-	--
PL43	1.0	2.0	5	2 $\times$ 30	0.018 $\pm$ 0.005	+	-
PL44	1.0	2.0	5	2 $\times$ 30	0.017 $\pm$ 0.007	-	--
PL45	1.0	2.0	5	2 $\times$ 30	0.017 $\pm$ 0.002	+	-
PL46	2.0	0.5	5	2 $\times$ 30	0.020 $\pm$ 0.008	+	+
PL47	2.0	0.5	5	2 $\times$ 30	0.013 $\pm$ 0.004	++	++
PL48	2.0	0.5	5	2 $\times$ 30	0.019 $\pm$ 0.004	+	+
PL49	2.0	0.5	5	2 $\times$ 30	0.019 $\pm$ 0.003	+	-
PL50	2.0	0.5	5	2 $\times$ 30	0.017 $\pm$ 0.003	+	+
PL51	2.0	0.5	5	2 $\times$ 30	0.013 $\pm$ 0.003	+	+
PL52	2.0	0.5	5	2 $\times$ 30	0.016 $\pm$ 0.003	+	+
PL53	2.0	0.5	5	2 $\times$ 30	0.017 $\pm$ 0.008	-	-
PL54	2.0	1.0	5	2 $\times$ 30	0.022 $\pm$ 0.011	++	+
PL55	2.0	1.0	5	2 $\times$ 30	0.048 $\pm$ 0.027	+	-

\*The polymer was also in the ultrasound bath. For the other samples, only the sucrose-chloroform solution was sonicated, and it was mixed with the PBSu afterwards.

**Table 6.** *Thickness, and microscopic and macroscopic features of different types of PBsu films prepared with the BF method. ++=very homogeneous/honeycomb-like, +=moderately homogeneous, -=moderately heterogeneous, --=very heterogeneous.*

SAMPLE CODE	CONCENTRATION (% W/V)	VOLUME (ML)	SURFAC-TANT CON-CENTRATION (% W/W)	HUMID-ITY (%)	THICKNESS ( $\mu\text{M}$ )	HOMO-GENE-ITY	OPTICAL MICRO-SCOPE
BF1	1.0	1.5	1	82	0.033 $\pm$ 0.005	--	--
BF2	1.0	2	1	76	0.029 $\pm$ 0.007	--	--
BF3	2.0	0.5	1	84	0.021 $\pm$ 0.002	--	--
BF4	2.0	1.0	1	65	0.029 $\pm$ 0.004	--	--
BF5	1.0	1.5	3	84	0.046 $\pm$ 0.010	--	--
BF6	1.0	2	3	76	0.066 $\pm$ 0.007	--	--
BF7	2.0	0.5	3	80	0.017 $\pm$ 0.012	-	-
BF8	2.0	1.0	3	79	0.051 $\pm$ 0.018	-	-
BF9	1.0	1.5	5	83	0.063 $\pm$ 0.011	-	-
BF10	1.0	2	5	82	0.080 $\pm$ 0.007	-	-
BF11	2.0	0.5	5	83	0.014 $\pm$ 0.002	++	++
BF12	2.0	1.0	5	81	0.075 $\pm$ 0.028	--	--
BF13	1.0	1.5	7	78	0.044 $\pm$ 0.033	-	-
BF14	1.0	2	7	81	-	--	--
BF15	2.0	0.5	7	82	0.016 $\pm$ 0.004	+	+
BF16	2.0	1.0	7	80	0.045 $\pm$ 0.002	-	--
BF17	1.0	0.5	3	83	0.016 $\pm$ 0.001	--	-
BF18	1.0	0.5	3	84	0.022 $\pm$ 0.001	--	--
BF19	2.0	0.5	3	84	0.017 $\pm$ 0.004	+	+
BF20	2.0	0.5	3	84	0.019 $\pm$ 0.003	+	+
BF21	1.0	0.5	5	84	0.017 $\pm$ 0.006	+	-
BF22	1.0	0.5	5	82	0.016 $\pm$ 0.002	-	-
BF23	2.0	0.5	5	84	0.020 $\pm$ 0.003	+	+
BF24	2.0	0.5	5	82	0.017 $\pm$ 0.002	++	++
BF25	1.0	0.5	5	83	0.026 $\pm$ 0.005	-	-
BF26	1.0	0.5	5	82	0.017 $\pm$ 0.001	+	+
BF27	2.0	0.5	5	84	0.019 $\pm$ 0.006	++	+
BF28	2.0	0.5	5	83	0.020 $\pm$ 0.005	++	+
BF29	2.0	0.5	5	81	0.018 $\pm$ 0.003	+	+
BF30	2.0	0.5	5	83	0.018 $\pm$ 0.002	+	++
BF31	2.0	0.5	5	83	0.019 $\pm$ 0.003	+	+
BF32	2.0	0.5	5	82	0.016 $\pm$ 0.004	+	++
BF33	2.0	0.5	5	82	0.016 $\pm$ 0.004	++	+
BF34	2.0	0.5	5	82	0.015 $\pm$ 0.002	-	+
BF35	2.0	0.5	5	78	0.017 $\pm$ 0.004	++	+
BF36	2.0	0.5	5	81	0.024 $\pm$ 0.001	-	-
BF37	2.0	0.5	5	88	0.017 $\pm$ 0.003	--	-
BF38	2.0	0.5	5	87	0.019 $\pm$ 0.004	--	-
BF39	2.0	0.5	5	84	0.017 $\pm$ 0.003	--	-
BF40	2.0	0.5	5	78	0.018 $\pm$ 0.003	+	+
BF41	2.0	0.5	5	81	0.018 $\pm$ 0.004	++	++
BF42	2.0	0.5	5	79	0.018 $\pm$ 0.003	++	+
BF43	2.0	0.5	5	80	0.016 $\pm$ 0.001	++	+
BF44	2.0	0.5	-	76	0.046 $\pm$ 0.031	--	--
BF45	2.0	0.5	-	83	0.042 $\pm$ 0.024	--	--
BF46	2.0	0.5	-	80	0.041 $\pm$ 0.016	--	--
BF47	2.0	0.5	-	84	0.031 $\pm$ 0.008	--	--
BF48	2.0	0.5	-	83	0.040 $\pm$ 0.025	--	--
BF49	2.0	0.5	-	83	0.031 $\pm$ 0.020	--	--
BF50	2.0	0.5	-	80	0.024 $\pm$ 0.009	--	--
BF51	2.0	0.5	-	84	0.026 $\pm$ 0.006	--	--
BF52	2.0	0.5	-	83		--	--
BF53	2.0	0.5	-	84		--	--
BF54	2.0	0.5	-	79		--	--
BF55	2.0	0.5	-	83		--	--

Figure 10 summarizes the thicknesses of the most promising films prepared by the PL- and BF-method as well as their control films. From the figure, it can be seen that the 2 % PBSu BF and 2 % PBSu PL films were the ones showing the highest reproducibility. The 1 % PBSu PL films also had better thickness than the control films (prepared in the absence of porogen), but as can be seen from the larger standard deviation, they had more variation than the two mentioned earlier. All the control films had very large standard deviations and they were also often too thick to be used as BM substrates.

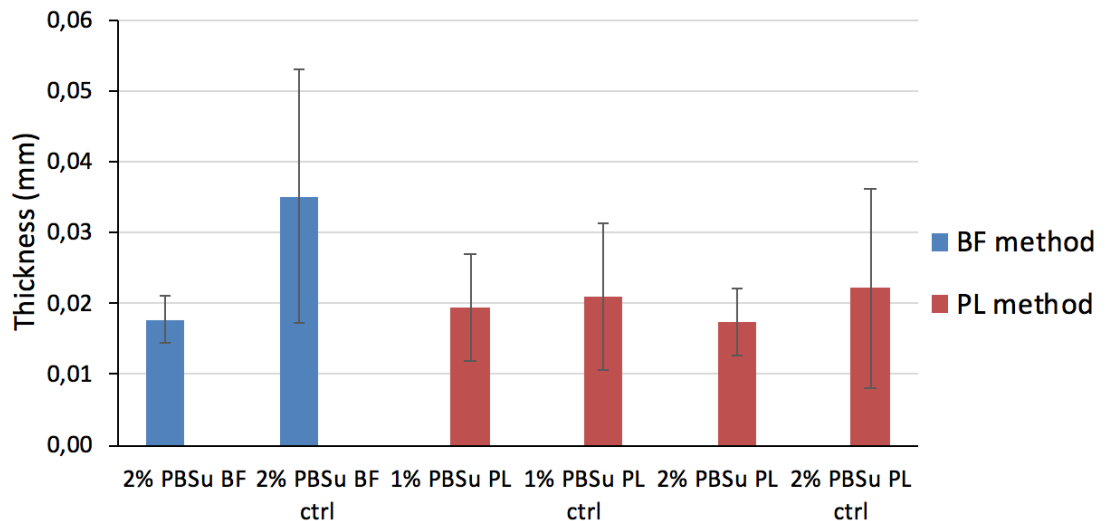


**Figure 10.** The thicknesses and standard deviations of the chosen BF and PL films.

The thinner BF films with surfactant and PL films with sucrose were all also easily handled with tweezers, which is important for future surgical implantation. It can be deduced that these would be better suited for BM substrates than the control films.

#### 4.1.2 Surface structure and porosity

The macro and micro structure of the film surface can affect the cell behaviour in cell culture, so it plays an important role in retinal tissue engineering. The first step in assessing these properties was to check the homogeneity of the film with a naked eye. The focus was to detect differences in the film opacity and whether the film was smooth or if it was wrinkled. The second step was to image films with the optical microscope to identify the presence and distribution of pores. The results from these observations are listed in the Table 5 and Table 6. The Figure 11 shows examples of the optical microscopy images of different types of samples.

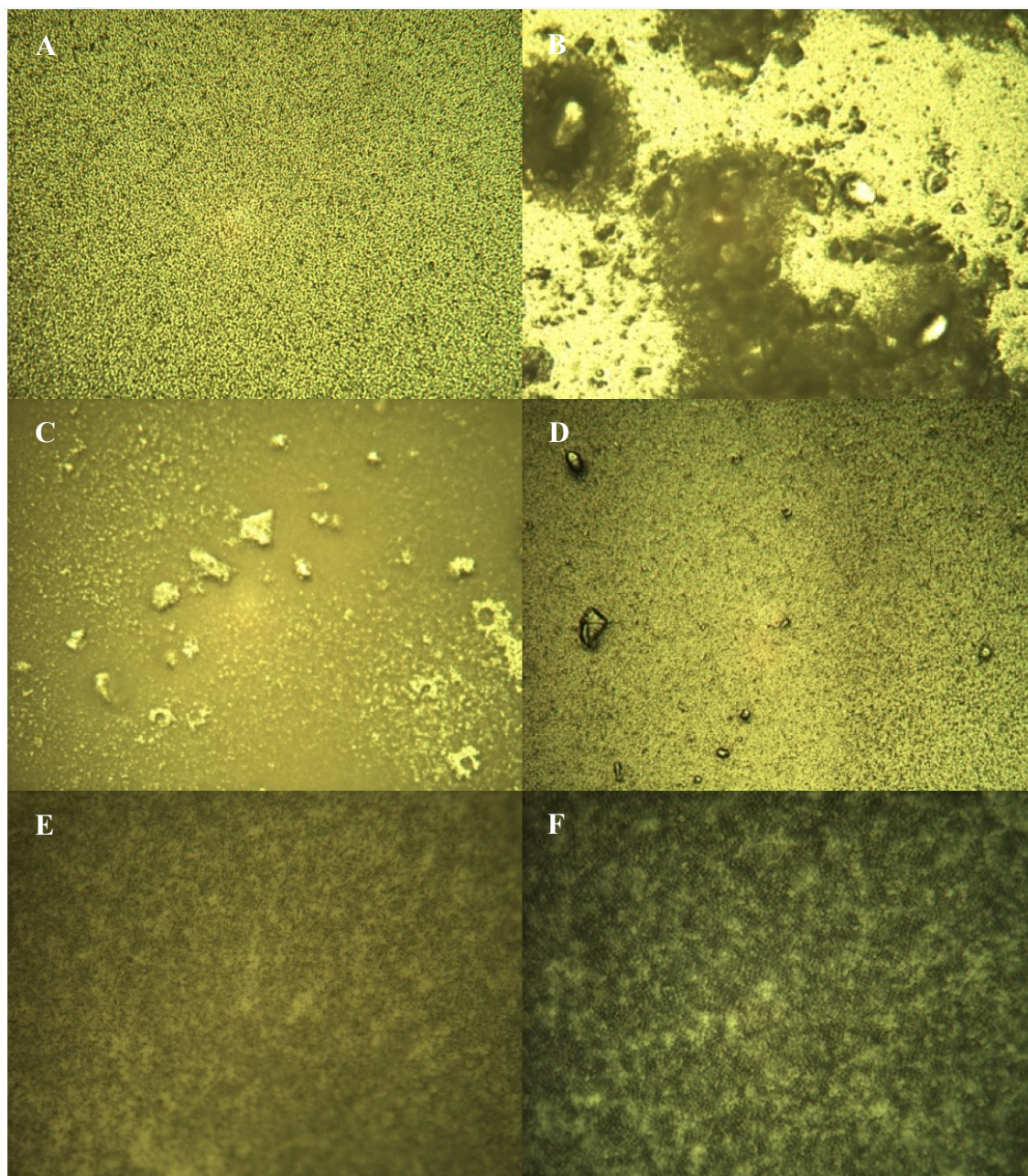


**Figure 11.** Examples of the optical microscopy images with  $20\times$  magnification of different types of films. A=2 % PBSu w/ 0.5 ml casting volume. B=2 % PBSu w/ 0.5 ml casting volume and 25 % sucrose. C=1 % PBSu w/ 2 ml casting volume and 5 % sucrose. D=2 % PBSu w/ 0.5 ml casting volume and 5 % sucrose. E and F=2 % PBSu w/ 0.5 ml casting volume and 5 % DOPE. Films A-D were cast in RH % of 30-55 % while E and F were cast in RH % of  $82 \pm 3$  %.

Image 11A is an image of the 2 % PBSu PL ctrl. There were small-sized features, resembling pores, homogeneously distributed through the material, but no large pores that could be detected at that magnification. The image 11B of a sample with 25 % sucrose on the other hand shows large pores where the sucrose particles were aggregated. The samples in the images 11C and 11D contained a significantly lower amount of aggregates, since

they only have 5 % sucrose and the sucrose-chloroform solution was sonicated in an ultrasound bath. However, some smaller aggregates can still be observed inside the polymer film that did not leach out when washed with water. In 11E and 11F a HC structure can be clearly seen all over the film. Unfortunately, the 2 % PBSu BF ctrl films were so thick and opaque that it was impossible to image them with an optical microscope. Even without optical microscopy imaging, it was visible to the naked eye that these had a very heterogeneous surface structure. Also, even though some of the 2 % PBSu BF films had the HC structure that was desired, not all replicates did. This was most likely due to slight changes in the humidity, the temperature and the speed of the fan in the humidity chamber. This suggests that much more refined and stable conditions are needed in order for this method to be reliably reproducible for this type of linear aliphatic polymer.

After the most potential films were chosen according to their thicknesses and optical microscopy images, their surface topography was imaged by AFM. This was completed in order to see their surface structure even more clearly and to determine the Arithmetic mean of surface roughness ( $R_a$ , Figure 14). However, AFM imaging is very time-consuming, and the data can be affected by unpredictable factors such as vibration, noise and electrical interference from other devices. Because of this, the samples to be imaged were chosen carefully. Examples of these images are seen in Figure 13: Week 0.

The surface topography of 2 % PBSu PL films was not significantly different from that of 2 % PBSu PL ctrl films. This could be due to density differences between the polymer solution and the solid sucrose particles. This can lead to the sucrose particles sinking to the bottom of the film while casting so there are not that many pores formed on the film surface. (Liao et al. 2002) The sucrose aggregates present in the optical microscope images are not seen on the AFM images, which suggests that they are stuck inside the polymer film not causing roughness on the film surface. Increasing the polymer concentration would increase the viscosity of the solution, which could solve this problem (Stenzel et al. 2006). A higher sucrose concentration could also result in more porous films. The fact that the sucrose solution was allowed to settle  $2 \times 60$  min before casting the films also resulted in some of the sucrose particles and aggregates to sink to the bottom of the vial. This combined with the fact that only the supernatant was used, lead to a loss of some sucrose particles, which could also play a part in the similarity of the surface structures. It also means that the exact concentration of the sucrose in the films is unknown. These results suggest that a better way to stop the sucrose particles from aggregating that will not result in losing any of the porogen is needed.

The 2 % PBSu BF and 2 % PBSu BF ctrl films, on the other hand, were shown to have a completely different surface structure. The 2 % PBSu BF film had a HC-like topography (Figure 12), which to the best of my knowledge, has not been seen before on materials prepared from this polymer. This HC was found to be slightly uneven in certain places, but there was still some kind of HC structure seen all over the film. These pores were somewhat similar in shape, and their pore diameter was around  $4 \mu\text{m}$ . This is in the range

that was found ideal (4-5  $\mu\text{m}$ ) by Calejo et al on poly(L-D-lactide) (PLDLA) films prepared with the BF method for RPE cell culture (Calejo et al. 2016). This pore size range can be considered optimal, expectedly ensuring high permeability while preventing the migration of differentiated hESC-RPE cells across the film as these cells have shown thicknesses of 7-15  $\mu\text{m}$  when cultured on biomaterials (Sorkio et al. 2014).

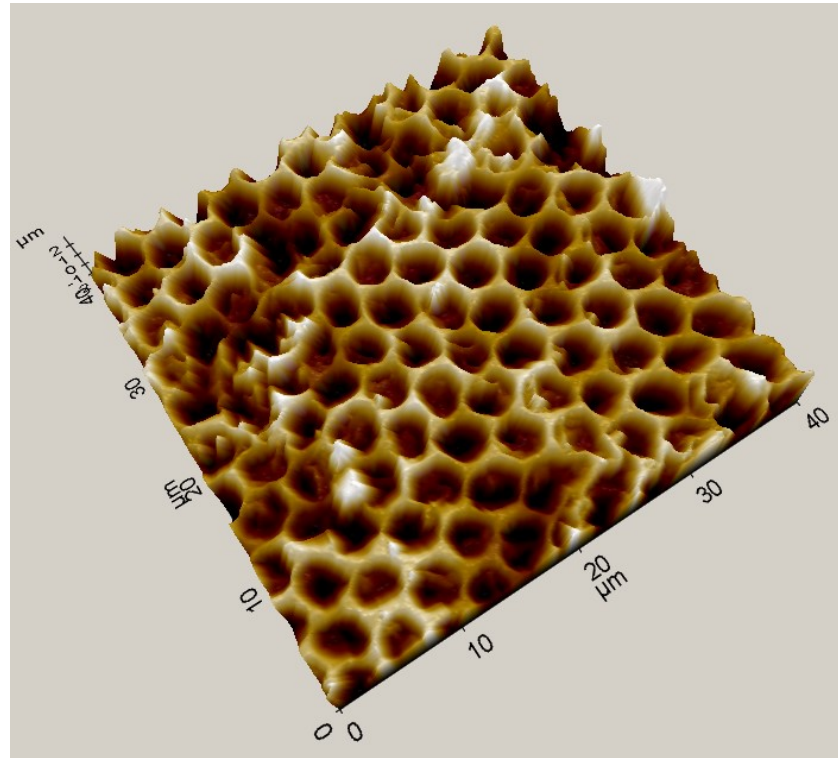


**Figure 12.** An AFM image of the 2 % PBSu BF HC structured film with a pore size of  $\sim 4 \mu\text{m}$

Unlike the 2 % PBSu BF films, the 2 % PBSu BF ctrl films had large, unorganized pores, distributed unevenly across the film surface. These pores also differed significantly in shape and size, in the range 1-10  $\mu\text{m}$ , hence expectedly not preventing migration of hESC-RPE cells across the film. The differences between these two films are caused by the surfactant decreasing the surface tension, which therefore prevents the water droplets from coalescing on the solvent surface. This enables the HC structure formation, while without the surfactant large water droplets are formed before the solvent is evaporated, which then leads to larger, more unorganized pores. (Fukuhira et al. 2006)

Film roughness varied significantly between samples (Figure 14, 0w). The 2 % PBSu BF film had clearly the highest surface roughness, while its control film had a roughness that was only slightly higher than the films' prepared by the PL method. The HC-structured PLDLA films with a pore diameter of 5  $\mu\text{m}$  were found to have  $R_a$  of  $\sim 0.90 \mu\text{m}$  while the commercial PET films had  $R_a$  of  $\sim 0.45 \mu\text{m}$  (Calejo et al. 2017). The 2 % PBSu BF film surface roughness appears to be between these two and even slightly closer to that of the PLDLA film. The effect of surface roughness in cell culture is not fully understood since

many different factors affect the cell adhesion. Typically, it is thought that cells adhere better on smoother surfaces, but it has also been proposed that filopodia that directly adheres to the surface irregularities would be responsible for the initial cell attachment. This means that smooth surfaces reduce the filopodia formation and therefore result in decreased adhesion and flattened cells. (Zhu et al. 2004)

### **4.1.3 *In vitro* stability of PBSu films**

Hydrolysis series was completed to see if the film preparation technique and the film surface structure would affect the film degradation or if there would even be any degradation detected during the 16-week series. The AFM images of the film surface, the  $R_a$ , the water absorption of the film and the film weight were the four factors used to study the stability of the PBSu films *in vitro*. The Figure 13 shows the AFM images of the films after different hydrolysis times. The first time point was at 2 weeks, but no significant mass loss or changes in the surface structure were detected at this time. For that reason, only the subsequent time points were imaged by AFM, as shown in Figure 13.

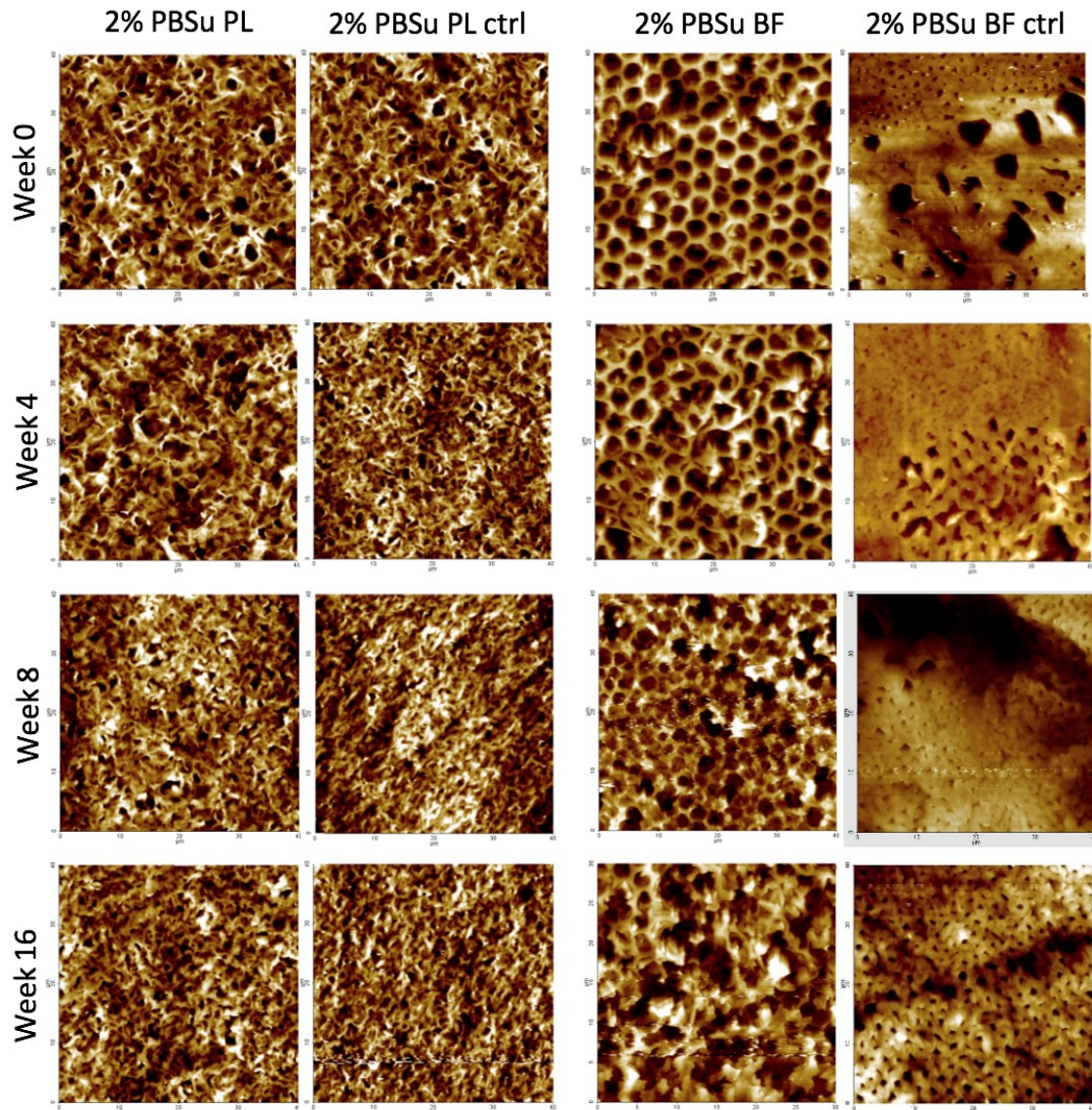


**Figure 13.** AFM images of different samples at different time points of the hydrolysis series. Scanned image area =  $40 \times 40 \mu\text{m}$ .

The 2 % PBSu PL and the 2 % PBSu PL ctrl films had similar surface structures that did not change significantly with incubation time. This is likely due to the fact that these samples were prepared in room humidity and the films are more uniform across the z-axis than BF films, with the exception of the presence of the small pores formed by particulate leaching. As such, the lower layers of the film that are exposed due to erosion reveal similar surface features and  $R_a$  values to the topmost layer, and the differences become insignificant.

Also, their surface roughness decreased at a similar rate from the original roughness of  $\sim 15 \mu\text{m}$  to the final roughness of  $\sim 8\text{-}10 \mu\text{m}$  during the 16 weeks. This suggests that there might not be any significant differences in the degradation rates between these two films and that the use of the sucrose particles does not significantly affect the film surface topography or the surface roughness.

As shown in Figure 13, samples prepared by BF in the presence and absence of DOPE reveal significantly different surface topography. Differences are also seen at the different incubation time points. The 2 % PBSu BF film has a decent HC structure that is not perfect all over the film though. After 4 weeks of hydrolysis the HC structure seems to be partly lost, possibly due to surface erosion. Nevertheless, after 8 weeks and especially after 16 weeks the 2 % PBSu BF films showed significant changes in the surface structure and at the end of the series the HC was barely detectable, due to exposure of the lower, less organized, layers of the film.

The 2 % PBS BF ctrl films' surface structure varied greatly within each film. They had unorganized pores, that differed in size (1-10  $\mu\text{m}$ ), distributed unevenly across the film surface. These variations can be clearly seen in Figure 13 week 0 and week 4 images. This makes it difficult to draw any conclusions about the changes in the surface structure during the hydrolysis series. These samples were also significantly challenging to image, possibly due to their highly heterogeneous surface structure that included large pores. This is why there were no additional images that could be used to compare the possible changes in the surface structure.

The 2 % PBSu BF film surface roughness decreased slightly during the first 8 weeks, but after that there was a noticeable drop from  $\sim 0.60 \mu\text{m}$  to  $\sim 0.44 \mu\text{m}$ . Despite this, its roughness still stayed clearly higher than the other films studied throughout the series. This suggests that the specific topography and high roughness of 2 % PBSu BF films could affect cell adhesion, proliferation and growth even after a few months of culture.

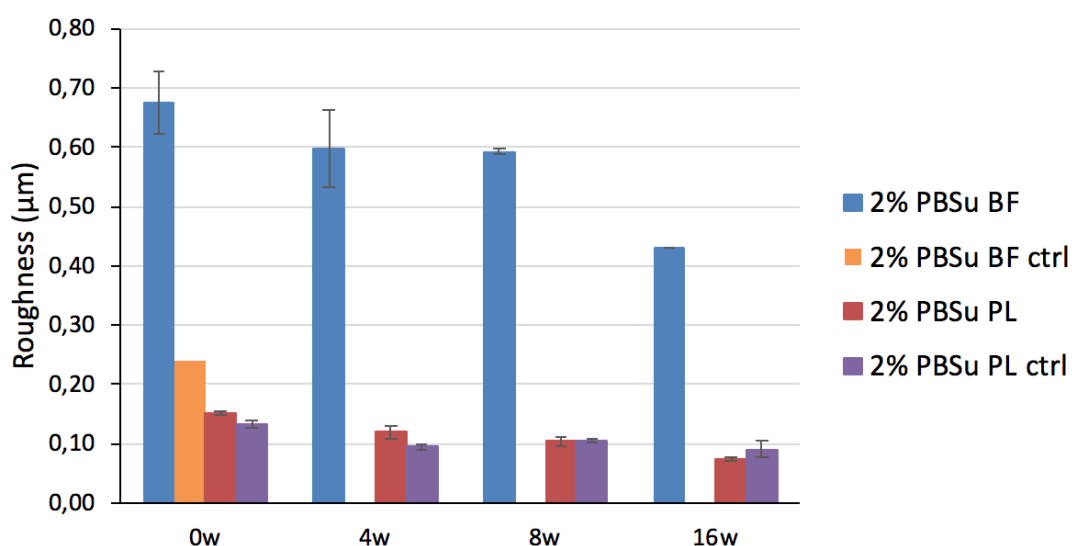


**Figure 14.** *The Arithmetic means of the film surface roughness ( $R_a$ ).*

The water absorption of the PL films is shown in Figure 15. The large standard deviations imply that there are not necessarily any significant differences between the different types of PL films. The films started to break at the 8-week time point and by 16 weeks some of them broke in very small pieces when handled, which made the weighing process difficult

or even impossible in some cases. This also partly explains the increase in the error bars at that time point, since eliminating the excess water from the materials became more challenging and some of the small pieces could also get lost during the weighing.

At the first look it appears that the BF films might absorb slightly more water than the PL films (Figure 16, Figure 15), which could be explained by their more porous surface structure. Also, the BF films' water absorptions seem to differ a bit more from each other than those of the PL films', but the large error bars make both of these differences quite insignificant. Similarly to the PL films, the BF films prepared with surfactant started to break after 8 weeks as well, even though not as severely as the PL films. The control BF films without surfactant were found to be the most durable films and also the easiest to handle, most likely due to them being the thickest ones of all the films.

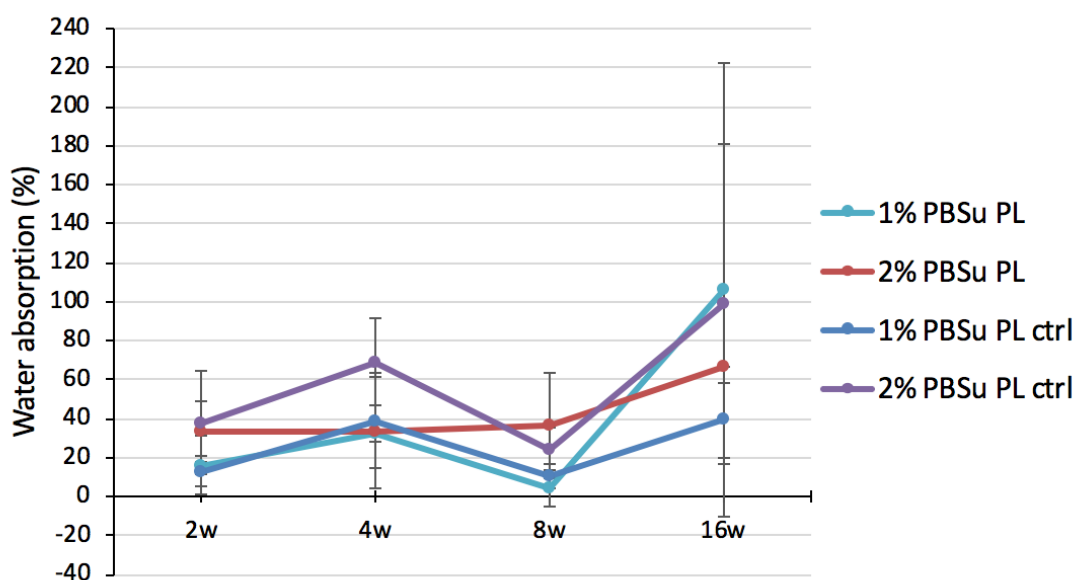


**Figure 15.** *The water absorptions of the PL films over time in TRIS buffer at 37 °C.*

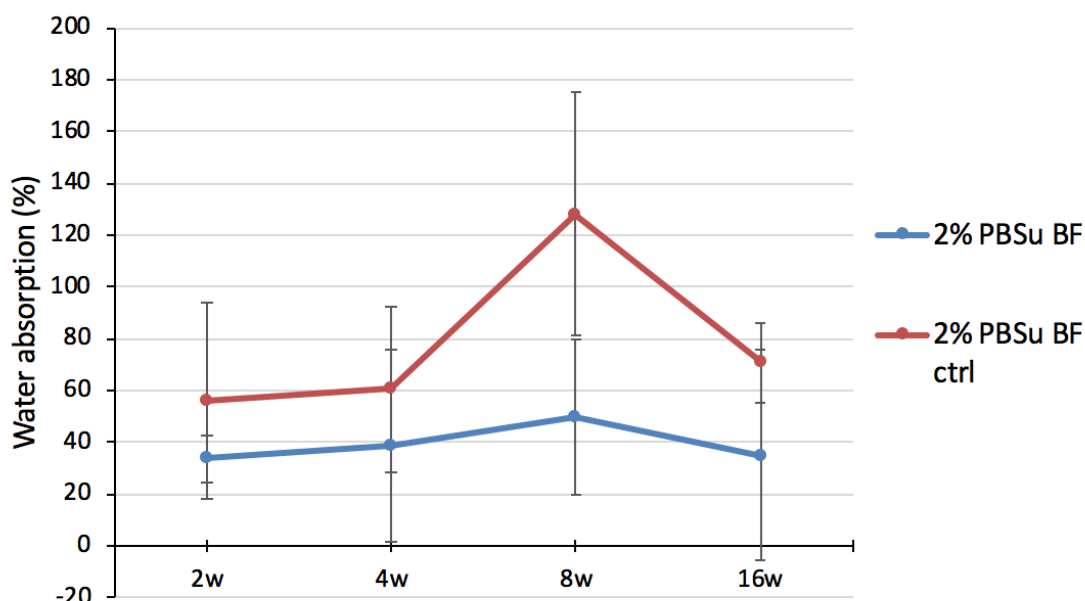


**Figure 16.** *The water absorption of the BF films over time in TRIS buffer at 37 °C.*

Mass loss values estimated for the PL films were also generally associated with relatively large standard deviations (Figure 17), which makes it impossible to say whether any mass loss has happened during the 16-week test period. The standard deviations of the PL method films became larger at 8 weeks, which is when the films started to break. The increased error could be explained by the fact that the static film pieces were very difficult to handle, and some small pieces could get lost during the weighing process. Also, the pieces weighed only around 0.5-1 mg, so even small changes or errors in the weighing would cause big differences.

Apart from the week 2, the measurement errors in the mass changes of the BF films were not particularly prominent (Figure 18). Especially at the 16-week time point, the standard deviation values were very small, which implies that the 2 % PBSu BF and the 2 % PBSu BF ctrl films' masses have decreased by about 10 % during the hydrolysis series. Quite surprisingly, however, there were not any differences seen between the control and the BF films. Even though the results for the BF method films are relatively constant, they cannot be used to draw any conclusions about the differences between the two manufacturing methods due to the significant errors in the results of the PL method films.

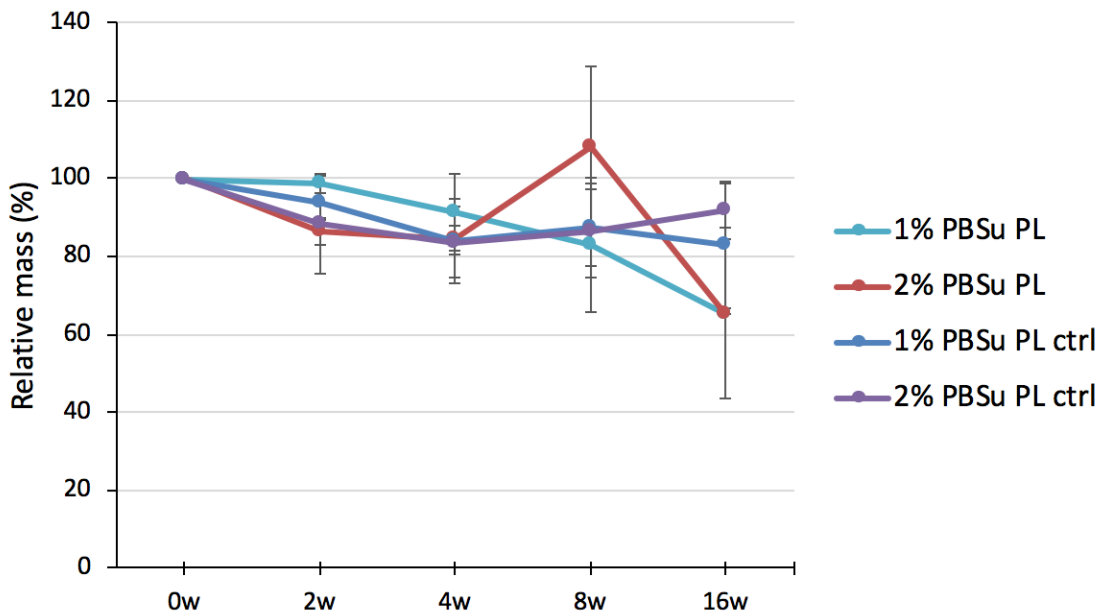


**Figure 17.** The mass loss of the PL films over time in TRIS-buffer at 37 °C.

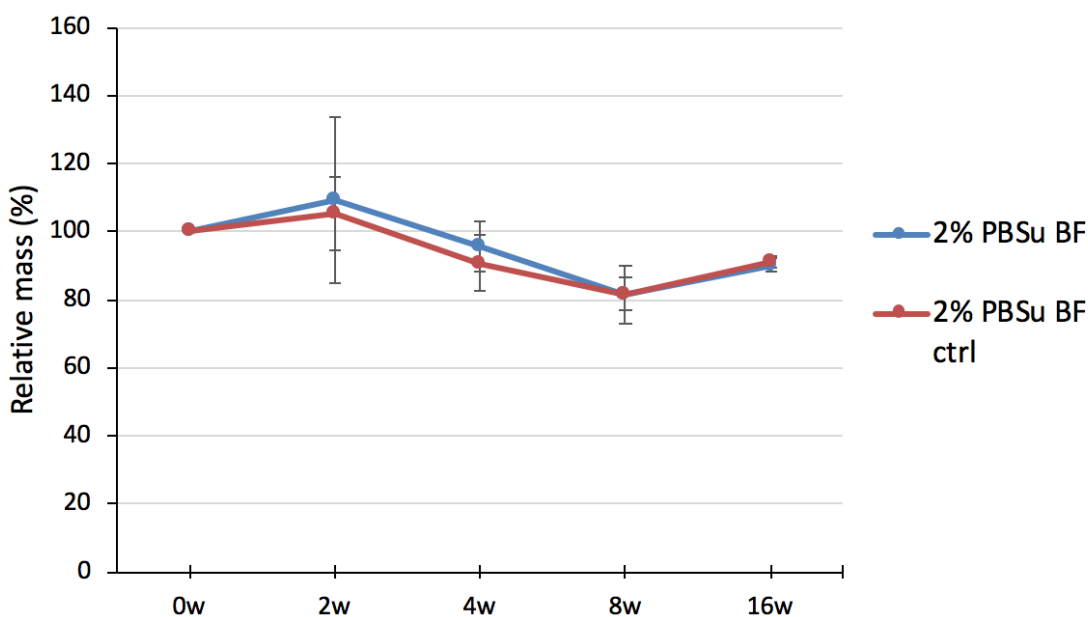


**Figure 18.** The mass loss of the BF films over time in TRIS-buffer at 37 °C.

The large standard deviations made analysing the results quite challenging. In future experiments using a larger sample size may make the mass measurements more reliable, since the small measurement errors would not be as significant anymore. In addition, using gas permeation chromatography for determining the polymer's molecular weight at different time points of the hydrolysis series would be beneficial, as it would show the polymer degradation in more detail. The use of gas permeation chromatography was not possible for this study due to a malfunction of the device.

#### 4.1.4 Film wettability

The water contact angle measurements showed that the addition of sucrose to the PL films had only a minor effect on the hydrophilicity of the films. Conversely, the usage of DOPE in the BF method increased the hydrophilicity of the films significantly and it also caused the WCA to decrease rapidly over time while it stayed quite constant on all the other films (Figure 19, Figure 20). The water contact angles of the 2 % PBSu BF films were measured before and after washing the DOPE away from the films to see if the surfactant left in the film would affect its hydrophilicity. There were only small differences between the two, but the wettability of the films increased fast within the 12 s of the measurement even after all the surfactant was washed away. Removing the surfactant mainly affected the standard deviations by reducing them to half of what they were before the washing (Figure 19 and Figure 20 show the results for the films after washing).

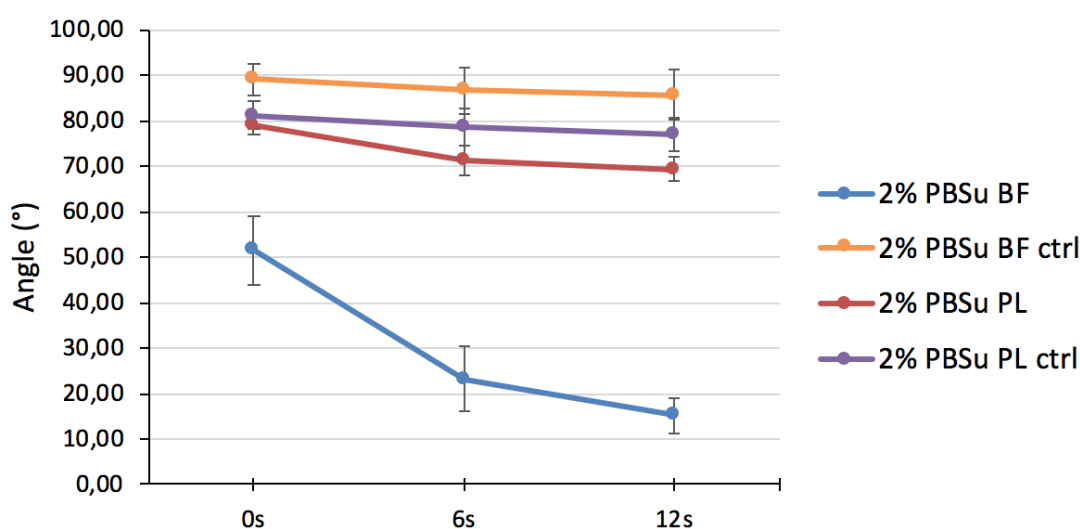


**Figure 19.** The water contact angles of the films at time points of 0s (as soon as the drop was placed on the film), 6s and 12s.

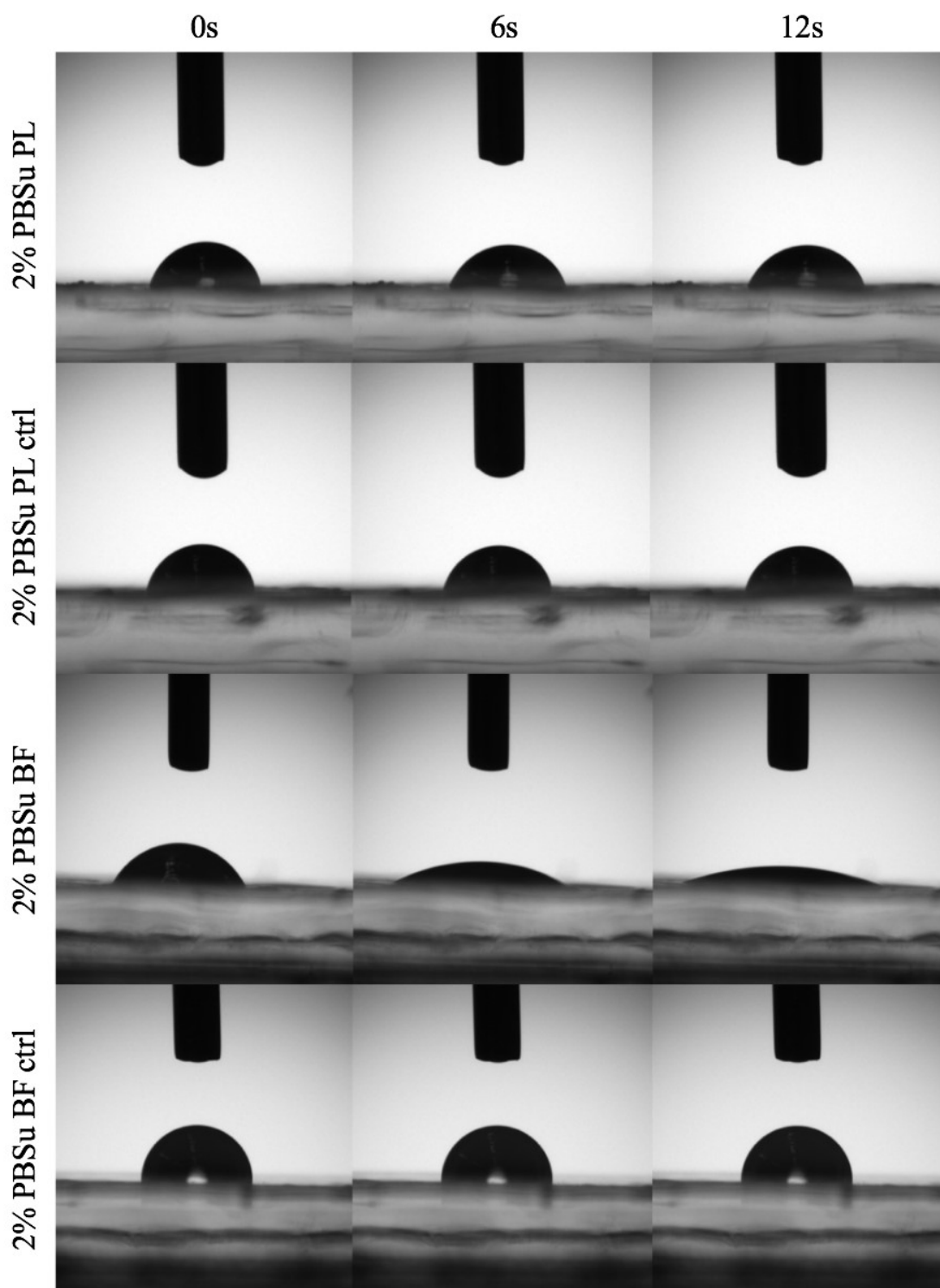


**Figure 20.** Images of the water droplets on different types of films during the water contact angle measurements at time points of 0s (as soon as the drop was placed on the film), 6s and 12s.

According to Wenzel's theory an increase in the surface roughness will result in a more hydrophilic surface (Wenzel 1936). This would seem to be the case with the HC structured films. However, another theory has been introduced according to which the surface

chemical composition can be changed during the BF process. During the BF method, the hydrophilic parts of the polymer tend to position themselves around the water droplets. This would cause the pores to be more hydrophilic while the hydrophobic parts of the polymer could end up on the film surface between the pores. This change in the chemical composition would decrease the surface free energy and lead to higher hydrophobicity and higher results in the WCA measurements. (Stenzel & Davis 2003; Ke et al. 2010; Galeotti et al. 2010; Heng et al. 2013) As can be concluded from these theories, the porous surface contact angles obey quite complex laws and are not necessarily proportional to the surface composition. The experimental values of the WCA measurements actually are subject to water or air inside the pores. So, depending on the polymer used and the pore size of the HC it is possible for the water to penetrate the pores which will lower the WCA results. (Stenzel et al. 2006) This and the increased surface roughness in the HC structured films could explain the significantly lower contact angles they showed compared to the other films.

The PLDLA films with a HC surface structure that had a similar pore size to the 2 % PBSu BF film, had initial WCAs of 120-125° compared to the 50-55° measured in this study. (Calejo et al. 2016) This shows that the PBSu HC structured films are much more hydrophilic. Thus, since the film hydrophilicity and wettability play an important role in cell adhesion and proliferation, it would seem that the HC structured 2 % PBSu BF films might have potential to work better in the cell culture studies than the other films studied. (Arima & Iwata 2007)

#### **4.1.5 Electrical resistance**

The results measured from the electrical resistance measurements were multiplied by the film surface area exposed in the slider (0.031 cm<sup>2</sup>). The final results are shown in Figure 21. When taking the standard deviations into consideration, there are not any significant differences seen between the 2 % PBSu PL, 2 % PBSu PL ctrl and 2 % PBSu BF films. The only sample differing from the others is the 2 % PBSu BF ctrl film for which the resistance detected was significantly lower. This is unexpected since the film was considerably thicker than all the other films. However, this could be caused by the presence of big pores in this heterogeneous film surface. Overall, the electrical resistance for all the films is low enough for them to be used as BM substitutes, since the mature hESC-RPE has an electrical resistance of 300-350 Ohm\*cm<sup>2</sup>, which makes the resistance through the PBSu films comparatively small (Vaajasaari et al. 2011).

Calejo et al. noticed a difference in the electrical resistance of films with different pore sizes all prepared by the BF method. The PLDLA films with a similar thickness and pore size to the 2 % PBSu BF film had an electrical resistance of 30-50 Ohm\*cm<sup>2</sup> compared to the ~70 Ohm\*cm<sup>2</sup> measured in this study. (Calejo et al. 2016) As noted before, this does not make a big difference in the films' performance in practice since the mature hESC-RPE will be the main resisting factor.

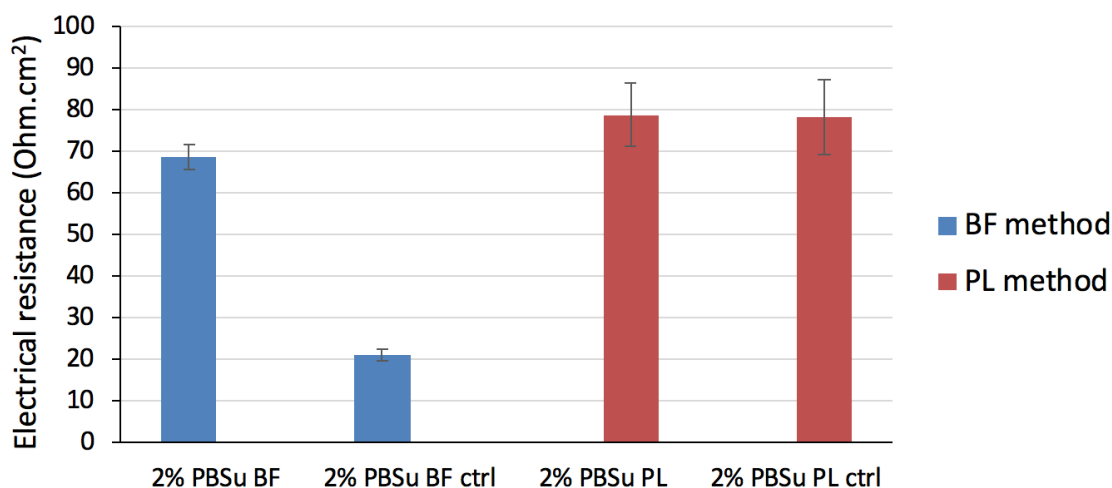


**Figure 21.** *The electrical resistances through the films.*

The 2 % PBSu BF film showed the properties that were desired for the hESC-RPE cell culture in this study. This sample was found to be significantly homogeneous, and to have appropriate thickness ( $0.018 \pm 0.003 \mu\text{m}$ ) for the application in retinal tissue engineering. In addition, the high wettability of the surface makes it appealing for cell adhesion, whereas the presence of an even HC topography across the film surface may facilitate the anchorage of cells through extending filopodia. The material did not hinder the flow of ions from one side to the other, as determined by the electrical resistance measurements. For all these reasons, this sample was chosen to be studied further in studies investigating the adhesion of hESC-RPE. The results of the culture are described in the following chapter. For comparison, the 2 % PBSu PL film was also chosen for the cell culture even though it did not fulfil all the requirements placed for the BM substitutes. Using this in addition to the BF film was expected to give more information about the influence of the film porosity and surface topography on hESC-RPE adhesion and viability.

## 4.2 Cell culture

The aim was to study the RPE cell viability and adhesion on plain PBSu and PET films as well as films coated with collagen IV and laminin mixture during a 5-day culturing period. The appearances of different proteins were investigated in order to study the cell adhesion and functionality on different film types.

Surface wettability and roughness have been found to be important factors that affect the cell adhesion and proliferation on biomaterial surfaces. It has been shown that cells adhere better on hydrophilic surfaces, but as said, also surface topography can affect the cell behaviour considerably (Arima & Iwata 2007). Even if smooth surfaces could decrease the filopodia formation (Zhu et al. 2004), cells have been proven to spread better on substrates with a relatively low surface roughness. This confirms that a specific surface topography improves the cell adhesion and proliferation. (Ranella et al. 2010) The 2 %

PBSu BF films with HC surface structure expressed high roughness values compared to the other films. However, Calejo et al. observed that dip-coating the films with ECM proteins decreased the surface roughness of the film. (Calejo et al. 2017) Therefore, coating the membranes with collagen IV and laminin could decrease the roughness values slightly in addition to providing ECM protein coating for the cells to adhere, resulting in surface that would enhance cell attachment. The 2 % PBSu PL films, on the other hand, were found to be relatively smooth, which could cause problems with formation of the filopodia extensions resulting in flattened cells (Zhu et al. 2004).

Cells typically adhere relatively poorly to synthetic polymers, since they naturally adhere to specific ECM protein sequences at FAs. The most common peptide motif of ECM proteins to which cells can adhere is Arg-Gly-Asp (RGD). Amongst others, this sequence is also found in laminin. (Wheeldon et al. 2011) Laminin and Collagen IV are also present in the basement membrane of the RPE in the natural BM. Since both of these are used as coating proteins in this study, this would suggest that the cells would adhere better on the coated films.

#### 4.2.1 Cell viability

Cell viability testing by PrestoBlue™ reagent was done on days 1, 2 and 5. Figure 22 shows the sample results after subtracting the control's absorbance. When considering the standard deviations of the measurements, there are not any big differences in cell viability between different days, different films or whether there was a protein coating or not.

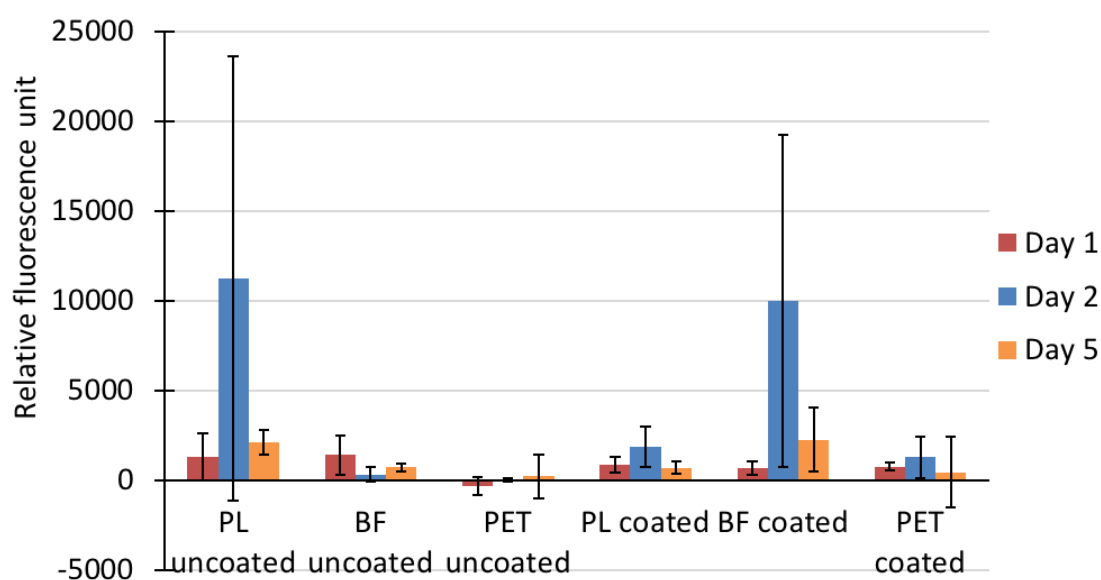


**Figure 22.** *The metabolic activity during in vitro culture as measured by Presto-Blue™ analysis after 1, 2 and 5 days of culture.*

The reliability of the results may have been affected by the few number of replicates used in cell culture. If there were more replicates, it would be easier to see if the results for one film differs drastically from the others, thus it could be disregarded from the final results. Also attaching the films to the inserts could have improved the results and decreased the standard deviations by preventing the films from curling up, therefore leading to more stable membranes for the cells to attach. Also the amount of the PrestoBlue™ medium used for the PET membranes differed from the amount used for the sample films, which could also have an effect on the results. This would be fixed if the sample films were attached to the inserts in the same way as the PET films, which would result in all the films having the same surface area used for the cell culturing. Furthermore, another way to measure cell viability could be used in addition to PrestoBlue™ testing. This could be done for example by using the LIVE/DEAD® Viability/Cytotoxicity Kit that stains the live cells green and the dead cells red, and imaging them with fluorescence microscopy.

#### **4.2.2 Immunostaining**

The proteins to be stained by IF were chosen specifically to give more information about the cell adhesion and the ability of the cells to form ECM. Since vinculin plays an important role in cell adhesion by crosslinking the actin cytoskeleton to talin at FAs, both vinculin and actin were chosen to be stained. The actin formation also indicates the presence of the forces needed for example for cell migration (Tojkander et al. 2012). Collagen IV, laminin and fibronectin were also stained because they are important ECM proteins that are present in the RPE basement membrane of the BM. They have also been shown to improve the formation of FAs and therefore to affect the cell viability and adhesion (Wheeldon et al. 2011; Calejo et al. 2016).

Collagen IV and laminin, used in this study to coat PL and BF films, were first immunostained and imaged by confocal microscopy, to investigate the distribution of the adsorbed proteins on the film surface. From the images in the Figure 23 it can be seen that the proteins have distributed nicely across the film surface in both of the films. When looked closely, a slight HC structure can be seen on the BF films where the proteins have arranged by the edges of the HC on the film. This is even more evident in Figure 26 on the coated BF film.

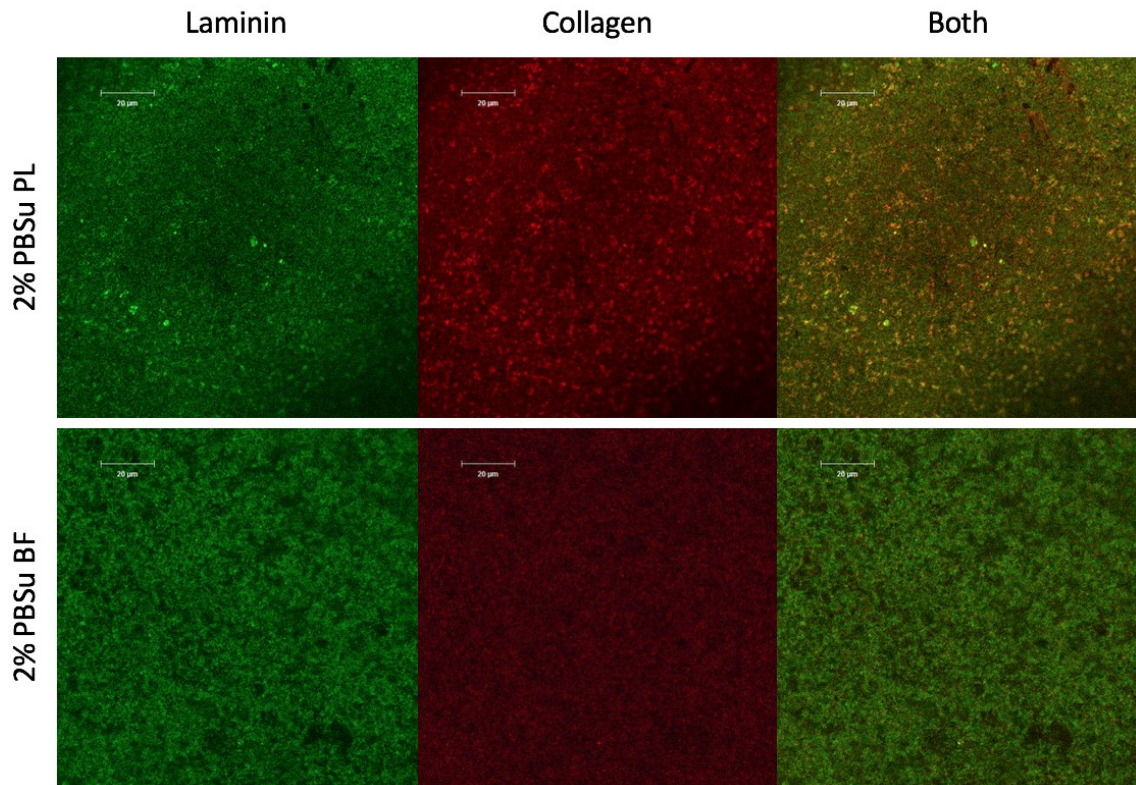


**Figure 23.** *Immunostained laminin- and collagen IV-coated films without any cells cultured on them, imaged by confocal microscopy.*

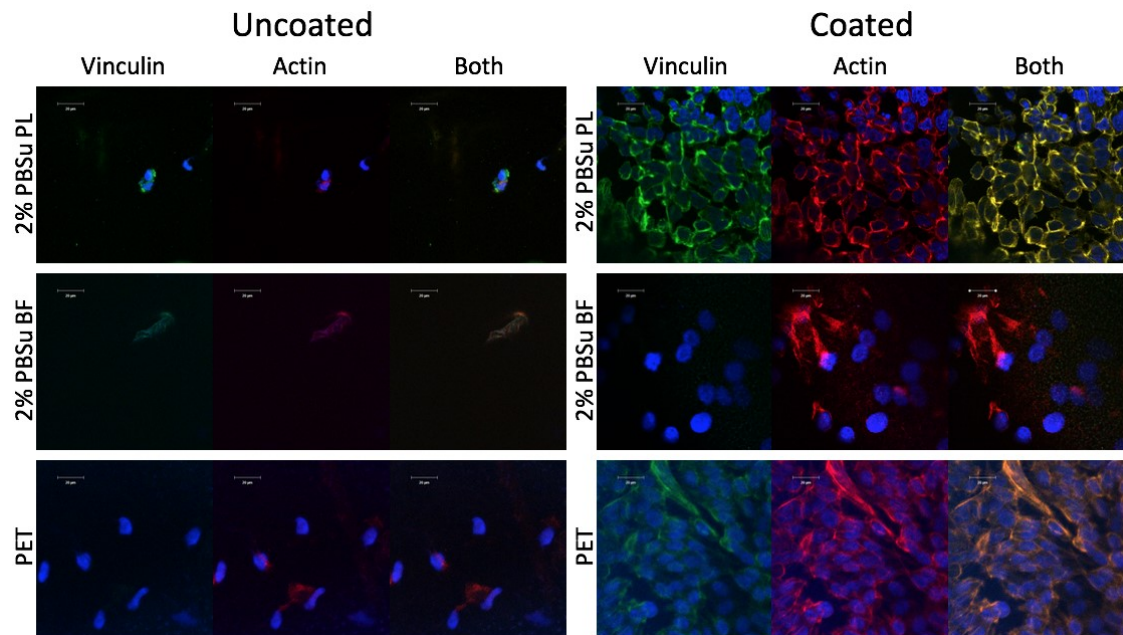
Calejo et al. found collagen IV to absorb on the rims of the HC structure as well as the inner walls and bottom of the pores of the PLDLA films. This was seen more clearly on the films with larger pore size. (Calejo et al. 2016) Similar results were also seen in this study on the 2 % PBSu BF films stained for collagen IV and laminin.

After cell culture, the immunostained films were imaged by confocal microscopy. These images give an idea of the number of cells and proteins present on the cultures, but they only show a small part of the film. Therefore, before taking the images, the entire films were checked on the microscope to see how much cells are actually growing on each of the films and how the cells are distributed across the film surface. These results are listed in Table 7. There are some conclusions that can already be drawn from these results: the cells grow significantly better on the coated films and the PL method films are the least suitable substrates for hESC-RPE cells, especially the uncoated ones.

**Table 7.** *The overall cell counts of the different films after 1 day and 5 days. +++=wide number of cells distributed quite evenly across the entire film surface, ++=a good number of cells either distributed evenly or in some more densely packed clusters, +=some cells, 0=no cells/very few cells.*

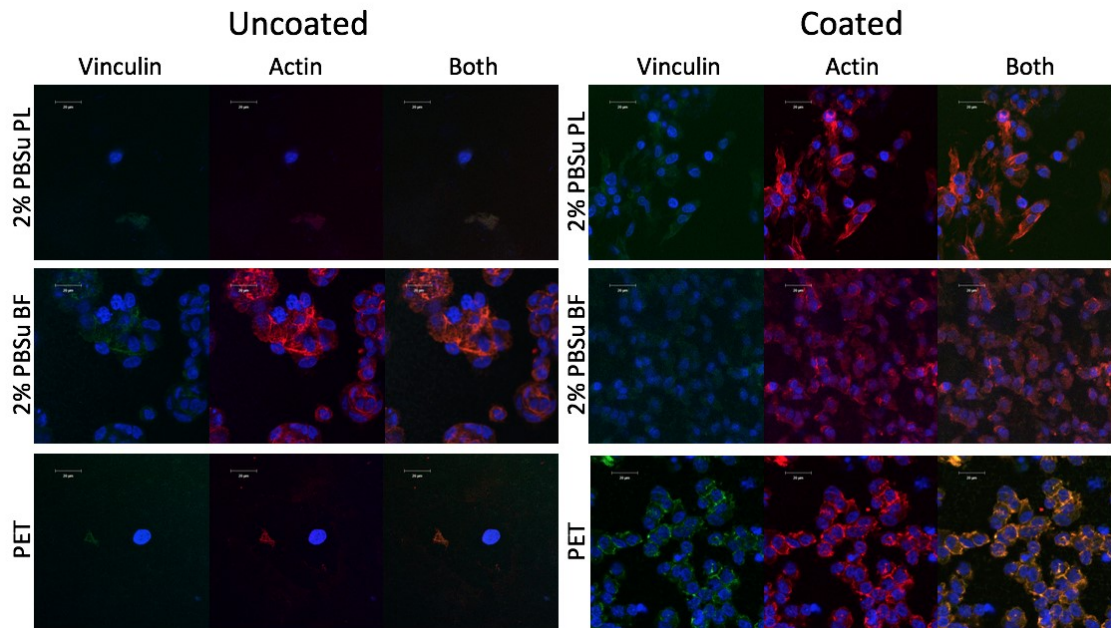
STAINING	FILM	DAY 1		DAY 5	
		UNCOATED	COATED	UNCOATED	COATED
VINCULIN/ ACTIN	PL	0	++	0	+++
	BF	+	++	++	+++
	PET	+	+++	0	+++
LAMININ/ COLLAGEN	PL	0	+++	0	++
	BF	+	+++	++	+++
	PET	+	+++	0	+++
FIBRONECTIN	PL	0	+	0	0
	BF	++	+++	++	+++
	PET	+		0	+++

Figure 24 shows the confocal microscopy images of the day 1 vinculin and actin stainings for both coated and uncoated films. It can be clearly seen that the coated films work significantly better for cell culture: there are considerably more cells present on the films and they have also secreted quite a lot of actin and vinculin. This is most likely due to the fact that laminin and collagen are found in the ECM and therefore the coating makes the films resemble more of the natural BM. Even though there are not many cells growing on the uncoated films, actin and vinculin could also be detected on these samples.



**Figure 24.** Vinculin and actin secretion by hESC-RPE cells 1 day after being cultured on uncoated, and collagen IV and laminin coated PL, BF and PET films. Green=vinculin, red=actin, blue=cell nucleus.

After 5 days, the results for vinculin and actin stained films had not changed much (Figure 25). There are slightly more cells growing in clusters on the uncoated BF film than there were before. There is also quite a lot of actin and vinculin formed by these clustered cells. The cells on all of the coated films seem quite similar after 5 days of culture, which suggests that PBSu as a material might be suitable for RPE cells since they keep on growing and forming FAs on all the PBSu films.



**Figure 25.** *Vinculin and actin secretion by hESC-RPE cells after 5 days of culturing on uncoated, and collagen IV and laminin coated PL, BF and PET films. Green=vinculin, red=actin, blue=cell nucleus.*

The vinculin and actin distribution seem to differ slightly between the film types. The location of actin filaments indicates that cells on the PL films are somewhat elongated and have a more fibroblast like shape, while the cells on the BF and PET films show more rounded shape, typical for RPE cells (particularly evident in Figure 25, coated films). This is in line with results published by Lim et al (Lim et al. 2004). They found that ARPE19 cells growing on smooth surfaces started to spread already after 1 day of culture, whereas cells on micropatterned surfaces were more rounded. After 1 and 3 weeks of culture, the cells grown on smooth surfaces showed a multilayer fibrillar cytoskeleton network, while cells on patterned surfaces did not show fibroblast-like phenotypes, and instead expressed a monolayered network of actin stress fibers. (Lim et al. 2004) It has also been shown that the elongated cells adhere stronger to the substrate in a wider focal contact area which results in them becoming flatter and losing their differentiated RPE morphology. (Opas et al. 1985) Maintaining the RPE cell morphology is especially important since it regulates processes and functions such as cell growth, differentiation and fibrosis (Bhatia et al. 1997; Casaroli-Marano et al. 1999; Lee et al. 2001)

The day 1 collagen and laminin stainings are shown in Figure 26. Again, the coated membranes show a lot more cell growth than the uncoated ones. It is not clear how much the cells produce collagen and laminin on the coated films, since the coating itself is also stained. Slightly more proteins are seen around the cells though (clearly seen on the coated PET film in Figure 26), but it is not possible to say whether those are produced by the cells or if the cells prefer the spots that have a thicker protein coating to begin with.

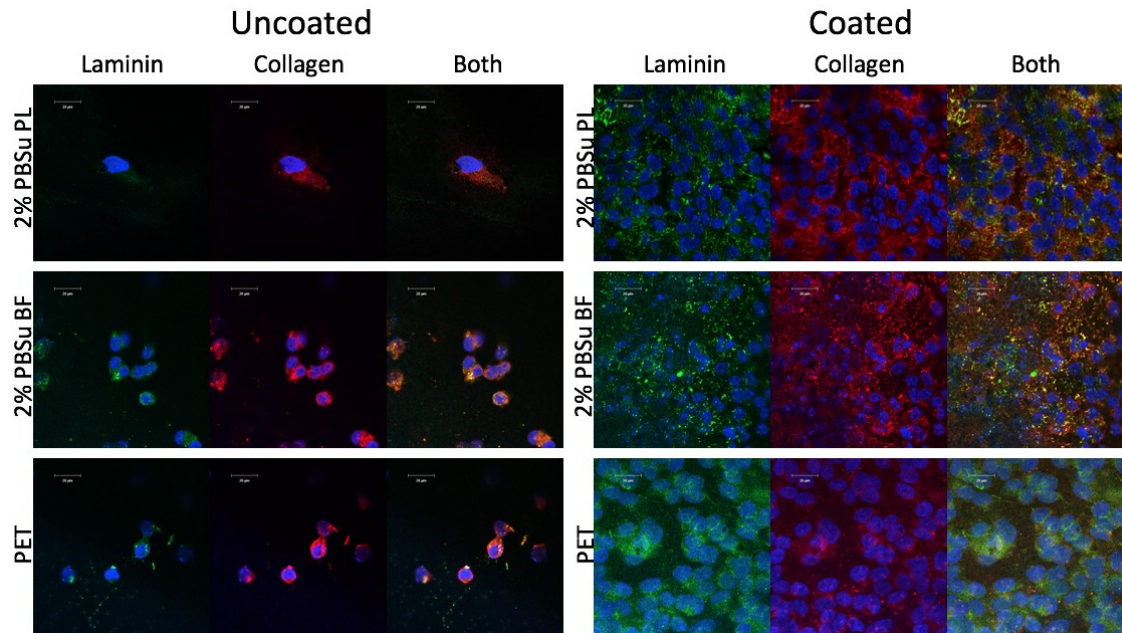


**Figure 26.** *Collagen IV and laminin seen 1 day after hESC-RPE cells have been cultured on uncoated, and collagen IV and laminin coated PL, BF and PET films. Green=laminin, red=collagen IV, blue=cell nucleus.*

The images of the 5-day samples in Figure 27 resemble day-1 samples. Both have few to no cells on the uncoated films that still form a small amount of laminin and collagen around the cells. The coated materials, on the other hand, demonstrate a high number of cells, and the protein coating is clearly seen.

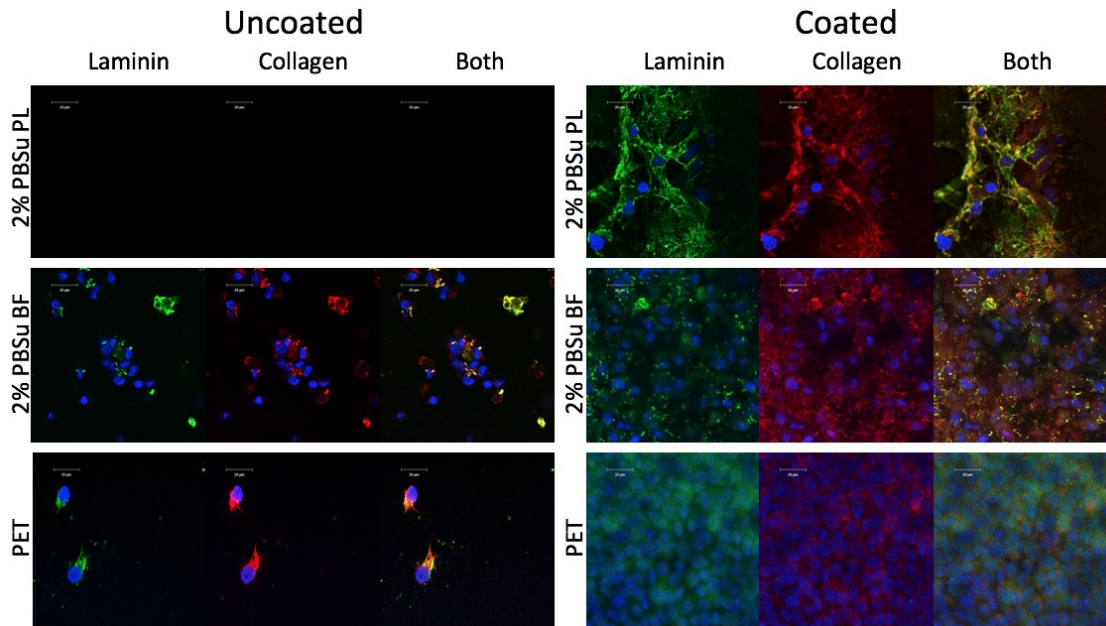


**Figure 27.** Collagen IV and laminin seen 5 days after hESC-RPE cells have been cultured on uncoated, and collagen IV and laminin coated PL, BF and PET films. Green=laminin, red=collagen IV, blue=cell nucleus.

The confocal images of the third ECM protein staining (fibronectin) for 1-day samples are seen in the Figure 28. Like stated with other proteins before, the cells grew better and also secreted more fibronectin on the coated membranes. Unfortunately, the coated PET membrane got lost during the staining process so there is no day 1 image of that.

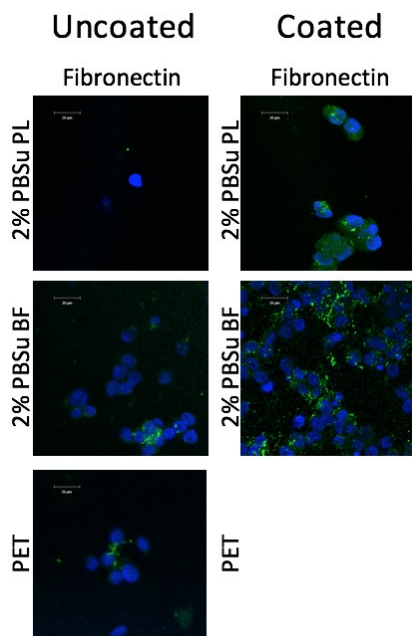


**Figure 28.** Fibronectin secretion by hESC-RPE cells 1 day after being cultured on uncoated, and collagen IV and laminin coated PL, BF and PET films. Green=fibronectin, blue=cell nucleus.

Again, the images look similar after 5 days (Figure 29). There are almost no cells growing on the PL films and on the uncoated PET film, whereas the uncoated BF film still has some cells growing on it. On the uncoated BF film, the formed fibronectin is clearly seen inside the cell cluster. The coated BF and PET films are filled with cells and they have formed a lot of fibronectin throughout the film. The coated PET film especially, clearly shows the formed fibronectin filaments.

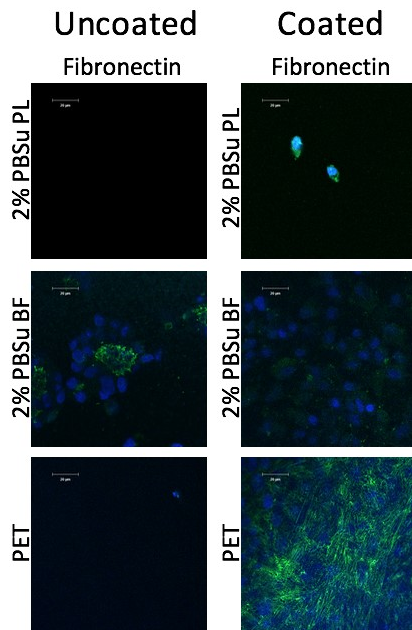


**Figure 29.** Fibronectin secretion by hESC-RPE cells after 5 days of culturing on uncoated, and collagen IV and laminin coated PL, BF and PET films. Green=fibronectin, blue=cell nucleus.

Previous studies have shown dip-coating with collagen and laminin to improve the hESC-RPE cell attachment to synthetic polymer membranes (Subrizi et al. 2012). This is in line with the results seen in confocal microscopy images in this study. All of the samples studied showed higher cell count growing on the ECM protein dip-coated films compared to the ones without the coating. They also secreted more vinculin, actin and fibronectin. As stated before, it is difficult to see the difference between the collagen IV and laminin secreted by the cells and the proteins present on the coating. However, these collagen and laminin stained films verify the adsorption of the coating proteins on the films.

Most of the RPE cell culture studies focus on investigating the RPE cell maturation by culturing the cells for a longer period of time (Xiang et al. 2014; Calejo et al. 2016; Calejo et al. 2017), and not many are found that study the cell adhesion in short-term cultures. The studies that were found, mostly determined the cell adhesion and viability by cell number instead of immunostaining the adhesion proteins (Tezcaner et al. 2003a; McLennan et al. 2017; White et al. 2017). Particularly, the effect of the surface topography on cell adhesion has been poorly studied.

The previous studies also mostly used immortalized RPE cell lines, primary cell lines or RPE cells of non-human origin (Opas 1985; Lu et al. 1999; Lu et al. 2001; Tezcaner et al. 2003b; Lim et al. 2004; Parapuram et al. 2009; McHugh et al. 2014; Baldwin et al. 2014; Lee et al. 2016; Teymouri et al. 2017), and to the best of my knowledge, the adhesion of hESC-RPE onto biomaterial surfaces has been scarcely studied so far. One disadvantage of the usage of these immortalized cell lines, such as ARPE19 cells is that they differ functionally from the native human RPE (Rabin et al. 2013). In addition to hESC-RPE resembling the native RPE better, the usage of hESCs to derive RPE cells provides an unlimited source of RPE cells. This makes hESC-RPE an interesting candidate for retinal tissue engineering, and clinical trials using them for treating AMD and Stargardt's Macular Dystrophy are ongoing (ClinicalTrials.gov).

For improving the results in the future, the optimal conditions for HC structure formation on PBSu films by the BF method could be determined in more detail since the surface topographies obtained in this study were not that constant. This would in turn make it easier to investigate the relationship between the film surface topography and the film properties, as well as cell adhesion, when all the samples would have the same surface structure. The degradation studies could be improved by using a larger sample size in order to make the weighing process easier and more reliable, and also by continuing the series for a longer period so the degradation could be seen more clearly. In addition, determining the polymer's molecular weight with gas permeation chromatography at different time points of the hydrolysis series would be beneficial, as it would show the polymer degradation even before there is any mass loss detected. For the cell culture part, it would be useful to attach the films to the inserts in order to prevent them from curling up and therefore giving the cells a stable and static substrate more comparable to the PET membranes. Conducting a LIVE-DEAD® Viability/Cytotoxicity analysis in addition to the PrestoBlue™ measurements would be highly beneficial for determining the cell viability in more detail. Also, it would have been useful to use more replicates of each film throughout the study in order to get more reliable results.

## 5. CONCLUSIONS

The aim of this thesis was to develop biodegradable porous scaffolds from PBSu as substrates for tissue engineering of hESC-RPE. For that purpose, it was deemed important that these films would allow the flow of nutrients, oxygen, ions and waste products that are essential for the RPE survival *in vitro* and if considering transplantation. Porous films were hence prepared, and the influence of different scaffold topographies – and associated properties – on hESC-RPE adhesion and behaviour was studied.

Films were prepared by solvent casting, using BF and PL methods to produce the porous surfaces. Various different PBSu concentrations, casting volumes, casting conditions, as well as surfactant and porogen concentrations were tested. Films with optimal thicknesses were obtained with 2 % PBSu with 5 % DOPE (BF method), 1 % PBSu with 5 % sucrose and 2 % PBSu with 5 % sucrose (PL method). The 2 % PBSu BF film was found to have a HC structured surface topography. However, the formation of the HC depended highly on the RH % and the airflow used during casting, and the surface topography was not always reproducible. This led to the occasional presence of less homogeneous topographies in some regions of some of the films, but there was still some kind of a HC structure all over the film. The pores were found to be similar in shape, and the pore diameter was around 4  $\mu\text{m}$ , which is expectedly appropriate for hESC-RPE cells. The 2 % PBSu BF ctrl films prepared without surfactant, on the other hand, were too thick to be used as a BM substitutes, and showed highly heterogeneous topography with pores differing in size in the range 1-10  $\mu\text{m}$ . On the contrary, the sucrose used as a porogen in the PL method did not affect the film surface topography notably.

*In vitro* stability studies demonstrated that all the films were generally stable for 8 weeks (2 % PBSu PL, 2 % PBSu PL ctrl, 2 % PBSu BF) or 16 weeks (2 % PBSu BF ctrl), with no significant mass loss detected during the series. The first signs of sample brittleness were observed after 8 weeks, which suggests that some degradation may have already happened during this time. No significant changes in the PL films' surface topography were detected during the hydrolysis series, while the 2 % PBSu BF film began to lose its HC structure already after 4 weeks of hydrolysis, and after 16 weeks the HC was barely detectable.

The WCA of the 2 % PBSu BF film was the lowest ( $\sim 50^\circ$ ) and differed drastically from the other samples. Interestingly, the WCA for this sample was also found to be time-dependent, decreasing to  $15^\circ$ , 12 s after the deposition of the water drop. For the other films, WCA was found between  $70-90^\circ$  throughout the test period, and no significant time-dependent changes were observed in the tested period.

There were no significant differences detected in the films' electrical resistances, except for the BF control film. The resistance for the BF control film was found to be significantly lower than the remaining samples, which could be due to the presence of big pores in the heterogeneous film surface. Nevertheless, the electrical resistance for all the films was found to be low enough for them to be used as BM substitutes, since the electrical resistance of mature hESC-RPE is much higher, which makes the resistance through the PBSu films comparatively insignificant.

Cell culture studies revealed significant differences in hESC-RPE cell adhesion between the uncoated films and the collagen IV and laminin coated films. The cells did not adhere well to the uncoated films, while the protein coating increased the adhesion by modifying the film surface to resemble more closely the natural BM. There were also differences in the cell adhesion between the different film types. Cells cultured on the coated PL films expressed somewhat elongated and fibroblast like shape with a multilayer fibrillar actin cytoskeleton network. The cells on the coated BF and PET films showed more rounded shape that is typical for RPE cells and there were also higher number of cells growing on these films.

This study showed that it is possible to prepare HC structured films of PBSu with the BF method. The results also demonstrated that it is possible for the hESC-RPE cells to adhere to PBSu, and that the HC surface topography as well as coating the films with collagen IV and laminin enhances the cell adhesion. This suggests that HC structured PBSu scaffolds can be promising candidates to be used as BM substitutes for RPE replacement therapy in the treatment of degenerative retinal diseases. Additional studies should be carried out in order to establish the effects of the PBSu substrates at later stages of hESC-RPE maturation, including morphological aspects, differentiation, gene expression and function. Future experiments should also explore the versatility of the BF method to produce films of different thickness and with tunable pore size and pore distribution, having in mind a broader scope of tissue engineering applications.

## 6. REFERENCES

- Afshari, F.T. & Fawcett, J.W. (2009). Improving RPE adhesion to Bruch's membrane, *Eye*, Vol. 23 pp. 1890.
- Almeida, L.R., Martins, A.R., Fernandes, E.M., Oliveira, M.B., Correlo, V.M., Pashkuleva, I., Marques, A.P., Ribeiro, A.S., Durães, N.F., Silva, C.J., Bonifácio, G., Sousa, R.A., Oliveira, A.L. & Reis, R.L. (2013). New biotextiles for tissue engineering: Development, characterization and in vitro cellular viability, *Acta Biomaterialia*, Vol. 9(9), pp. 8167-8181.
- Alves da Silva, M L, Crawford, A., Mundy, J.M., Correlo, V.M., Sol, P., Bhattacharya, M., Hatton, P.V., Reis, R.L. & Neves, N.M. (2010). Chitosan/polyester-based scaffolds for cartilage tissue engineering: Assessment of extracellular matrix formation, Vol. 6(3), pp. 1149-1157.
- Ambati, J. & Fowler, B. (2012). Mechanisms of Age-Related Macular Degeneration, *Neuron*, Vol. 75(1), pp. 26-39.
- Arai, K., Tanaka, M., Yamamoto, S. & Shimomura, M. (2008). Effect of pore size of honeycomb films on the morphology, adhesion and cytoskeletal organization of cardiac myocytes, *Colloids and Surfaces A: Physicochemical and Engineering Aspects*, Vol. 313-314 pp. 530-535.
- Arima, Y. & Iwata, H. (2007). Effect of wettability and surface functional groups on protein adsorption and cell adhesion using well-defined mixed self-assembled monolayers, *Biomaterials*, Vol. 28(20), pp. 3074-3082.
- Arphavasin, S., Singhatanadgit, W., Ngamviriyavong, P., Janvikul, W., Meesap, P. & Patntirapong, S. (2013). Enhanced osteogenic activity of a poly(butylene succinate)/calcium phosphate composite by simple alkaline hydrolysis, *Biomedical Materials*, Vol. 8(5), pp. 1-8.
- Baldwin, A.K., Cain, S.A., Lennon, R., Godwin, A., Merry, C.L.R. & Kielty, C.M. (2014). Epithelial–mesenchymal status influences how cells deposit fibrillin microfibrils, *Journal of cell science*, Vol. 127(1), pp. 158.
- Barthes, J., Özçelik, H., Hindié, M., Ndreu-Halili, A., Hasan, A. & Vrana, N.E. (2014). Cell Microenvironment Engineering and Monitoring for Tissue Engineering and Regenerative Medicine: The Recent Advances, *BioMed Research International*, Vol. 2014 pp. 921905.
- Bhatia, S.N., Yarmush, M.L. & Toner, M. (1997). Controlling cell interactions by micropatterning in co-cultures: hepatocytes and 3T3 fibroblasts, *Journal of Biomedical Materials Research*, Vol. 34(2), pp. 189-199.
- Bonilha, V.L. (2008). Age and disease-related structural changes in the retinal pigment epithelium, *Clinical ophthalmology (Auckland, N.Z.)*, Vol. 2(2), pp. 413-424.

- Booij, J.C., Baas, D.C., Beisekeeva, J., Gorgels, T G M F & Bergen, A.A.B. (2010). The dynamic nature of Bruch's membrane, *Progress in Retinal and Eye Research*, Vol. 29(1), pp. 1-18.
- Borges, E.R. & Pereira, N. (2011). Succinic acid production from sugarcane bagasse hemicellulose hydrolysate by *Actinobacillus succinogenes*, *Journal of industrial microbiology & biotechnology*, Vol. 38(8), pp. 1001-1011.
- Boulton, M.E. (2014). Studying melanin and lipofuscin in RPE cell culture models, *Experimental Eye Research*, Vol. 126 pp. 61-67.
- Brunner, C.T., Baran, E.T., Pinho, E.D., Reis, R.L. & Neves, N.M. (2011). Performance of biodegradable microcapsules of poly(butylene succinate), poly(butylene succinate-co-adipate) and poly(butylene terephthalate-co-adipate) as drug encapsulation systems, *Colloids and Surfaces B: Biointerfaces*, Vol. 84(2), pp. 498-507.
- Buchholz, D.E., Pennington, B.O., Croze, R.H., Hinman, C.R., Coffey, P.J. & Clegg, D.O. (2013). Rapid and efficient directed differentiation of human pluripotent stem cells into retinal pigmented epithelium, *Stem cells translational medicine*, Vol. 2(5), pp. 384-393.
- Burke, J.M. (2008). Epithelial phenotype and the RPE: Is the answer blowing in the Wnt? *Progress in Retinal and Eye Research*, Vol. 27(6), pp. 579-595.
- Calejo, M.T., Ilmarinen, T., Jongprasitkul, H., Skottman, H. & Kellomäki, M. (2016). Honeycomb porous films as permeable scaffold materials for human embryonic stem cell-derived retinal pigment epithelium, *Journal of Biomedical Materials Research Part A*, Vol. 104(7), pp. 1646-1656.
- Calejo, M.T., Ilmarinen, T., Skottman, H. & Kellomäki, M. (2018). Breath figures in tissue engineering and drug delivery: State-of-the-art and future perspectives, *Acta Biomaterialia*, Vol. 66 pp. 44-66.
- Calejo, M.T., Ilmarinen, T., Vuorimaa-Laukkanen, E., Talvitie, E., Hakola, H.M., Skottman, H. & Kellomäki, M. (2017). Langmuir-Schaefer film deposition onto honeycomb porous films for retinal tissue engineering, *Acta Biomaterialia*, Vol. 54 pp. 138-149.
- Carrasco, F., Pagès, P., Gámez-Pérez, J., Santana, O.O. & MasPOCH, M.L. (2010). Processing of poly(lactic acid): Characterization of chemical structure, thermal stability and mechanical properties, *Polymer Degradation and Stability*, Vol. 95(2), pp. 116-125.
- Casaroli-Marano, R.P., Pagan, R. & Vilaro, S. (1999). Epithelial-mesenchymal transition in proliferative vitreoretinopathy: intermediate filament protein expression in retinal pigment epithelial cells, *Investigative ophthalmology & visual science*, Vol. 40(9), pp. 2062-2072.
- Chaudhuri, J.B., Davidson, M.G., Ellis, M.J., Jones, M.D. & Wu, X. (2008). Fabrication of Honeycomb-Structured Poly(DL-lactide) and Poly(DL-lactide)-co-glycolide] Films and their Use as Scaffolds for Osteoblast-Like Cell Culture, *Macromolecular Symposia*, Vol. 272(1), pp. 52-57.

ClinicalTrials.gov <https://clinicaltrials.gov/ct2/home>.

Costa-Pinto, A., Vargel, I., Tuzlakoglu, K., Correlo, V.M., Sol, P.C., Faria, S., Piskin, E., Reis, R.L. & Neves, N.M. (2014). Influence of scaffold composition over in vitro osteogenic differentiation of hBMSCs and in vivo inflammatory response, *J Biomater Appl*, Vol. 28(9), pp. 1430-1442.

Curcio, C.A. & Johnson, M. (2013). Chapter 20 - Structure, Function, and Pathology of Bruch's Membrane, in: Ryan, S.J. et al. (ed.), *Retina (Fifth Edition)*, W.B. Saunders, London, pp. 465-481.

Davson, H. (1980). 5 - Retinal structure and organization, in: Davson, H. (ed.), *Physiology of the Eye (Fourth Edition)*, Academic Press, pp. 167-177.

Del Priore, L.V., Tezel, T.H. & Kaplan, H.J. (2006). Maculoplasty for age-related macular degeneration: Reengineering Bruch's membrane and the human macula, *Progress in Retinal and Eye Research*, Vol. 25(6), pp. 539-562.

Diniz, B., Thomas, P., Thomas, B., Ribeiro, R., Hu, Y., Brant, R., Ahuja, A., Zhu, D., Liu, L., Koss, M., Maia, M., Chader, G., Hinton, D.R. & Humayun, M.S. (2013). Sub-retinal Implantation of Retinal Pigment Epithelial Cells Derived From Human Embryonic Stem Cells: Improved Survival When Implanted as a Monolayer, *Investigative ophthalmology & visual science*, Vol. 54(7), pp. 5087-5096.

Eniwumide, J.O., Tanaka, M., Nagai, N., Morita, Y., de Bruijn, J., Yamamoto, S., Onodera, S., Kondo, E., Yasuda, K. & Shimomura, M. (2014). The Morphology and Functions of Articular Chondrocytes on a Honeycomb-Patterned Surface, *BioMed Research International*, Vol. 2014 pp. 10.

Escalé, P., Rubatat, L., Billon, L. & Save, M. (2012). Recent advances in honeycomb-structured porous polymer films prepared via breath figures, *European Polymer Journal*, Vol. 48(6), pp. 1001-1025.

Feeny, A.K., Tadarati, M., Freund, D.E., Bressler, N.M. & Burlina, P. (2015). Automated segmentation of geographic atrophy of the retinal epithelium via random forests in AREDS color fundus images, *Computers in Biology and Medicine*, Vol. 65 pp. 124-136.

Ferreira, L.P., da Cunha, B.P., Kuster, R.M., Pinto, J.C., Souza, M.N. & de Souza Junior, Fernando Gomes (2017). Synthesis and chemical modification of poly(butylene succinate) with rutin useful to the release of silybin, *Industrial Crops and Products*, Vol. 97 pp. 599-611.

Ferreira, L.P., Moreira, A.N., Pinto, J.C. & de Souza, F.G. (2015). Synthesis of poly(butylene succinate) using metal catalysts, *Polymer Engineering & Science*, Vol. 55(8), pp. 1889-1896.

Fujimaki, T. (1998). Processability and properties of aliphatic polyesters, 'BI-ONOLLE', synthesized by polycondensation reaction, *Polymer Degradation and Stability*, Vol. 59(1), pp. 209-214.

- Fukuhira, Y., Kaneko, H., Yamaga, M., Tanaka, M., Yamamoto, S. & Shimomura, M. (2008). Effect of honeycomb-patterned structure on chondrocyte behavior in vitro, *Colloids and Surfaces A: Physicochemical and Engineering Aspects*, Vol. 313-314 pp. 520-525.
- Fukuhira, Y., Kitazono, E., Hayashi, T., Kaneko, H., Tanaka, M., Shimomura, M. & Sumi, Y. (2006). Biodegradable honeycomb-patterned film composed of poly(lactic acid) and dioleoylphosphatidylethanolamine, *Biomaterials*, Vol. 27(9), pp. 1797-1802.
- Garcia, J.M., Mendonça, L., Brant, R., Abud, M., Regatieri, C. & Diniz, B. (2015). Stem cell therapy for retinal diseases, *World Journal of Stem Cells*, Vol. 7(1), pp. 160-164.
- Gigli, M., Fabbri, M., Lotti, N., Gamberini, R., Rimini, B. & Munari, A. (2016). Poly(butylene succinate)-based polyesters for biomedical applications: A review, *European Polymer Journal*, Vol. 75 pp. 431-460.
- Gigli, M., Negroni, A., Soccio, M., Zanaroli, G., Lotti, N., Fava, F. & Munari, A. (2012). Influence of chemical and architectural modifications on the enzymatic hydrolysis of poly(butylene succinate), *Green Chemistry*, Vol. 14(10), pp. 2885-2893.
- Goldmann, W.H. (2016). Role of vinculin in cellular mechanotransduction, *Cell biology international*, Vol. 40(3), pp. 241-256.
- Golji, J., Lam, J. & Mofrad, M. (2011). Vinculin activation is necessary for complete talin binding, *Biophysical journal*, Vol. 100 pp. 332-340.
- Gong, J., Sagiv, O., Cai, H., Tsang, S.H. & Del Priore, L.V. (2008). Effects of extracellular matrix and neighboring cells on induction of human embryonic stem cells into retinal or retinal pigment epithelial progenitors, *Experimental Eye Research*, Vol. 86(6), pp. 957-965.
- Gualandi, C., Soccio, M., Govoni, M., Valente, S., Lotti, N., Munari, A., Giordano, E., Pasquinelli, G. & Focarete, M.L. (2012). Poly(butylene/diethylene glycol succinate) multiblock copolyester as a candidate biomaterial for soft tissue engineering: Solid-state properties, degradability, and biocompatibility, *Journal of Bioactive and Compatible Polymers*, Vol. 27(3), pp. 244-264.
- Gualandi, C., Soccio, M., Saino, E., Focarete, M.L., Lotti, N., Munari, A., Moroni, L. & Visai, L. (2012). Easily synthesized novel biodegradable copolyesters with adjustable properties for biomedical applications, *Soft Matter*, Vol. 8(20), pp. 5466-5476.
- Gullapalli, V.K., Sugino, I.K. & Zarbin, M.A. (2008). Culture-induced increase in alpha integrin subunit expression in retinal pigment epithelium is important for improved re-surfacing of aged human Bruch's membrane, *Experimental eye research*, Vol. 86(2), pp. 189-200.
- Haiyan, L., Jiang, C., Amin, C. & Junying, W. (2005). in vitro Evaluation of Biodegradable Poly(butylene succinate) as a Novel Biomaterial, *Macromolecular Bioscience*, Vol. 5(5), pp. 433-440.

- Han, S.-, Kang, S.-, Kim, B.- & Im, S. (2005). A Novel Polymeric Ionomer as a Potential Biomaterial: Crystallization Behavior, Degradation, and In-Vitro Cellular Interactions, *Advanced Functional Materials*, Vol. 15(3), pp. 367-374.
- Hariraksapitak, P., Suwantong, O., Pavasant, P. & Supaphol, P. (2008). Effectual drug-releasing porous scaffolds from 1,6-diisocyanatohexane-extended poly(1,4-butylene succinate) for bone tissue regeneration, *Polymer*, Vol. 49(11), pp. 2678-2685.
- Haugsdal, J. & Sohn, E. (2013). Age-related macular degeneration: from one medical student to another, [EyeRounds.org](http://EyeRounds.org).
- Hongisto, H., Ilmarinen, T., Vattulainen, M., Mikhailova, A. & Skottman, H. (2017). Xeno- and feeder-free differentiation of human pluripotent stem cells to two distinct ocular epithelial cell types using simple modifications of one method, *Stem cell research & therapy*, Vol. 8.
- Hongisto, H., Jylhä, A., Nättinen, J., Rieck, J., Ilmarinen, T., Vereb, Z., Aapola, U., Beuerman, R., Petrovski, G., Uusitalo, H. & Skottman, H. (2017). Comparative proteomic analysis of human embryonic stem cell-derived and primary human retinal pigment epithelium, *Scientific reports*, Vol. 7.
- Hotaling, N.A., Khristov, V., Wan, Q., Sharma, R., Jha, B.S., Lotfi, M., Maminishkis, A., Simon, C.G. & Bharti, K. (2016). Nanofiber Scaffold-Based Tissue-Engineered Retinal Pigment Epithelium to Treat Degenerative Eye Diseases, *Journal of Ocular Pharmacology and Therapeutics*, Vol. 32(5), pp. 272-285.
- Hu, C., Tercero, C., Ikeda, S., Nakajima, M., Tajima, H., Shen, Y., Fukuda, T. & Arai, F. (2013). Biodegradable porous sheet-like scaffolds for soft-tissue engineering using a combined particulate leaching of salt particles and magnetic sugar particles, *Journal of Bioscience and Bioengineering*, Vol. 116(1), pp. 126-131.
- Hutmacher, D.W. (2000). Scaffolds in tissue engineering bone and cartilage, *Biomaterials*, Vol. 21(24), pp. 2529-2543.
- Jacquel, N., Freyermouth, F., Fenouillot, F., Rousseau, A., Pascault, J.P., Fuertes, P. & Saint-Loup, R. (2011). Synthesis and properties of poly(butylene succinate): Efficiency of different transesterification catalysts, *Journal of Polymer Science Part A: Polymer Chemistry*, Vol. 49(24), pp. 5301-5312.
- Janik, H. & Marzec, M. (2015). A review: Fabrication of porous polyurethane scaffolds, *Materials Science and Engineering: C*, Vol. 48 pp. 586-591.
- Janson, I.A. & Putnam, A.J. (2015). Extracellular matrix elasticity and topography: Material-based cues that affect cell function via conserved mechanisms, *Journal of Biomedical Materials Research Part A*, Vol. 103(3), pp. 1246-1258.
- Kaarniranta, K., Sinha, D., Blasiak, J., Kauppinen, A., Veréb, Z., Salminen, A., Boulton, M.E. & Petrovski, G. (2013). Autophagy and heterophagy dysregulation leads to retinal pigment epithelium dysfunction and development of age-related macular degeneration, *Autophagy*, Vol. 9(7), pp. 973-984.

- Kaewkong, P., Uppanan, P., Thavornyutikarn, B., Kosorn, W. & Janvikul, W. (2012). Chondrocyte Growth and Function on HPBS/HA Composite Scaffolds: Static Versus Dynamic Culture &nbsp; IPCBEE, Vol. 43 pp. 11-14.
- Kosorn, W., Thavornyutikarn, B., Phumsiri, B., Uppanan, P., Meesap, P. & Janvikul, W. (2010). Hydrolyzed Poly(Butylene Succinate) Scaffolds Coated with Bioactive Agent &nbsp; Journal of Metals, Materials and Minerals, Vol. 20(3), pp. 95-99.
- Leach, L.L., Croze, R.H., Hu, Q., Nadar, V.P., Clevenger, T.N., Pennington, B.O., Gamm, D.M. & Clegg, D.O. (2016). Induced Pluripotent Stem Cell-Derived Retinal Pigmented Epithelium: A Comparative Study Between Cell Lines and Differentiation Methods, Journal of ocular pharmacology and therapeutics : the official journal of the Association for Ocular Pharmacology and Therapeutics, Vol. 32(5), pp. 317-330.
- Lee, K., Kim, E.H., Oh, N., Tuan, N.A., Bae, N.H., Lee, S.J., Lee, K.G., Eom, C., Yim, E.K. & Park, S. (2016). Contribution of actin filaments and microtubules to cell elongation and alignment depends on the grating depth of microgratings, Journal of nanobiotechnology, Vol. 14(1), pp. 35.
- Lee, S.C., Kwon, O.W., Seong, G.J., Kim, S.H., Ahn, J.E. & Kay, E.D. (2001). Epitheliomesenchymal transdifferentiation of cultured RPE cells, Ophthalmic research, Vol. 33(2), pp. 80-86.
- Liao, C., Chen, C., Chen, J., Chiang, S., Lin, Y. & Chang, K. (2002). Fabrication of porous biodegradable polymer scaffolds using a solvent merging/particulate leaching method, Journal of Biomedical Materials Research, Vol. 59(4), pp. 676-681.
- Lim, J., Byun, S., Chung, S., Park, T., Hyun, Seo, J., Joo, C., Chung, H. & Cho, D. (2004). Retinal Pigment Epithelial Cell Behavior is Modulated by Alterations in Focal Cell-Substrate Contacts, Investigative Ophthalmology & Visual Science, Vol. 45(11), pp. 4210-4216.
- Lim, L.S., Mitchell, P., Seddon, J.M., Holz, F.G. & Wong, T.Y. (2012). Age-related macular degeneration, The Lancet, Vol. 379(9827), pp. 1728-1738.
- Lu, L., Yaszemski, M.J. & Mikos, A.G. (2001). Retinal pigment epithelium engineering using synthetic biodegradable polymers, Biomaterials, Vol. 22(24), pp. 3345-3355.
- Lu, L., Kam, L., Hasenbein, M., Nyalakonda, K., Bizios, R., Göpferich, A., Young, J.F. & Mikos, A.G. (1999). Retinal pigment epithelial cell function on substrates with chemically micropatterned surfaces, Biomaterials, Vol. 20(23), pp. 2351-2361.
- McCarthy, J.B., Vachhani, B. & Iida, J. (1996). Cell adhesion to collagenous matrices, Biopolymers, Vol. 40(4), pp. 371-381.
- McHugh, K.J., Tao, S.L. & Saint-Geniez, M. (2014). Porous poly(epsilon-caprolactone) scaffolds for retinal pigment epithelium transplantation, Investigative ophthalmology & visual science, Vol. 55(3), pp. 1754-1762.

- McLenachan, S., Hao, E., Zhang, D., Zhang, L., Edel, M. & Chen, F. (2017). Bioengineered Bruch's-like extracellular matrix promotes retinal pigment epithelial differentiation, *Biochemistry and Biophysics Reports*, Vol. 10 pp. 178-185.
- Meesap, P., Uppanan, P., Thavornnyutikarn, B., Kosorn, W. & Janvikul, W. (2010). Surface Hydrolyzed Poly(Butylene Succinate) Microsphere Incorporated Carboxymethylchitosan Scaffolds for Cartilage Tissue Engineering & Journal of Metals, Materials and Minerals, Vol. 20(3), pp. 107-111.
- Mikos, A.G., Thorsen, A.J., Czerwonka, L.A., Bao, Y., Langer, R., Winslow, D.N. & Vacanti, J.P. (1994). Preparation and characterization of poly(l-lactic acid) foams, *Polymer*, Vol. 35(5), pp. 1068-1077.
- Ngamviriyavong, P., Patntirapong, S., Janvikul, W., Arphavasin, S., Meesap, P. & Singhatanadgit, W. (2014). Development of poly(butylene succinate)/calcium phosphate composites for bone engineering, *Composite Interfaces*, Vol. 21(5), pp. 431-441.
- Nguyen, A.T., Sathe, S.R. & Yim, E.K. (2016). From nano to micro: topographical scale and its impact on cell adhesion, morphology and contact guidance, *Journal of physics. Condensed matter : an Institute of Physics journal*, Vol. 28(18), pp. 183001.
- Nishikawa, T., Arai, K., Hayashi, J., Hara, M. & Shimomura, M. (2002). "Honeycomb films": Biointerface for tissue engineering, *International Journal of Nanoscience*, Vol. 01(05), pp. 415-418.
- Oliveira, J.T., Correlo, V.M., Sol, P.C., Costa-Pinto, A.R., Malafaya, P.B., Salgado, A.J., Bhattacharya, M., Charbord, P., Neves, N.M. & Reis, R.L. (2008). Assessment of the Suitability of Chitosan/PolyButylene Succinate Scaffolds Seeded with Mouse Mesenchymal Progenitor Cells for a Cartilage Tissue Engineering Approach, *Tissue Engineering Part A*, Vol. 14(10), pp. 1651-1661.
- Oliveira, J.T., Crawford, A., Mundy, J.L., Sol, P.C., Correlo, V.M., Bhattacharya, M., Neves, N.M., Hatton, P.V. & Reis, R.L. (2011). Novel Melt-Processable Chitosan–Polybutylene Succinate Fibre Scaffolds for Cartilage Tissue Engineering, *Journal of Biomaterials Science, Polymer Edition*, Vol. 22(4-6), pp. 773-788.
- Opas, M. (1985). The focal adhesions of chick retinal pigmented epithelial cells, *Canadian journal of biochemistry and cell biology = Revue canadienne de biochimie et biologie cellulaire*, Vol. 63(6), pp. 553-563.
- Opas, M., Turksen, K. & Kalnins, V.I. (1985). Adhesiveness and distribution of vinculin and spectrin in retinal pigmented epithelial cells during growth and differentiation in vitro, *Developmental Biology*, Vol. 107(2), pp. 269-280.
- Parapuram, S.,K., Chang, B., Li, L., Hartung, R.,A., Chalam, K.,V., Nair-Menon, J.,U., Hunt, D.,Margaret & Hunt, R.,C. (2009). Differential Effects of TGF $\beta$  and Vitreous on the Transformation of Retinal Pigment Epithelial Cells, *Investigative Ophthalmology & Visual Science*, Vol. 50(12), pp. 5965-5974.

Purves, D. (2009). Vision, in: Berntson, G.G. & Cacioppo, J.T. (ed.), *Handbook of Neuroscience for the Behavioral Sciences*,

Rabin, D.M., Rabin, R.L., Blenkinsop, T.A., Temple, S. & Stern, J.H. (2013). Chronic oxidative stress upregulates Drusen-related protein expression in adult human RPE stem cell-derived RPE cells: a novel culture model for dry AMD, *Aging*, Vol. 5(1), pp. 51-66.

Ramrattan, R.S., van der Schaft, T. L., Mooy, C.M., de Bruijn, W.C., Mulder, P.G. & de Jong, P.T. (1994). Morphometric analysis of Bruch's membrane, the choriocapillaris, and the choroid in aging, *Investigative Ophthalmology & Visual Science*, Vol. 35(6), pp. 2857-2864.

Ranella, A., Barberoglou, M., Bakogianni, S., Fotakis, C. & Stratakis, E. (2010). Tuning cell adhesion by controlling the roughness and wettability of 3D micro/nano silicon structures, *Acta Biomaterialia*, Vol. 6(7), pp. 2711-2720.

Riera, M., Fontrodona, L., Albert, S., Ramirez, D.M., Seriola, A., Salas, A., Muoz, Y., Ramos, D., Villegas-Perez, M.P., Zapata, M.A., Raya, A., Ruberte, J., Veiga, A. & Garcia-Arumi, J. (2016). Comparative study of human embryonic stem cells (hESC) and human induced pluripotent stem cells (hiPSC) as a treatment for retinal dystrophies, *Molecular Therapy - Methods & Clinical Development*, Vol. 3 pp. 16010.

Rizzolo, L.J. (2014). Barrier properties of cultured retinal pigment epithelium, *Experimental Eye Research*, Vol. 126 pp. 16-26.

Rizzolo, L.J., Peng, S., Luo, Y. & Xiao, W. (2011). Integration of tight junctions and claudins with the barrier functions of the retinal pigment epithelium, *Progress in Retinal and Eye Research*, Vol. 30(5), pp. 296-323.

Schwartz, S.D., Tan, G., Hosseini, H. & Nagiel, A. (2016). Subretinal Transplantation of Embryonic Stem Cell-Derived Retinal Pigment Epithelium for the Treatment of Macular Degeneration: An Assessment at 4 Years, *Investigative ophthalmology & visual science*, Vol. 57(5), pp. 9.

Shadforth, A.M.A., George, K.A., Kwan, A.S., Chirila, T.V. & Harkin, D.G. (2012). The cultivation of human retinal pigment epithelial cells on Bombyx mori silk fibroin, *Biomaterials*, Vol. 33(16), pp. 4110-4117.

Shang, P., Stepicheva, N.A., Hose, S., Zigler, J.S. & Sinha, D. (2018). Primary Cell Cultures from the Mouse Retinal Pigment Epithelium, *JoVE*, (133), pp. e56997.

Simó, R., Villarroel, M., Corraliza, L., Hernández, C. & Garcia-Ramírez, M. (2010). The retinal pigment epithelium: Something more than a constituent of the blood-retinal barrier--implications for the pathogenesis of diabetic retinopathy. *Journal of Biomedicine & Biotechnology*, Vol. 2010.

Singhal, S. & Vemuganti, G.K. (2005). Primary adult human retinal pigment epithelial cell cultures on human amniotic membranes, *Indian journal of ophthalmology*, Vol. 53(2), pp. 109-113.

Skeie, J.M. (2010). Choroidal endothelial cell activation in age-related macular degeneration, University of Iowa.

Sorkio, A.E., Vuorimaa-Laukkanen, E.P., Hakola, H.M., Liang, H., Ujula, T.A., Valle-Delgado, J.J., Österberg, M., Yliperttula, M.L. & Skottman, H. (2015). Biomimetic collagen I and IV double layer Langmuir–Schaefer films as microenvironment for human pluripotent stem cell derived retinal pigment epithelial cells, *Biomaterials*, Vol. 51 pp. 257-269.

Sorkio, A. (2016). Biomaterial substrates and transplantation materials for human embryonic stem cell derived retinal pigment epithelial cells: Biomimetic approaches for retinal tissue engineering, University of Tampere; Tampere University Press.

Sorkio, A., Hongisto, H., Kaarniranta, K., Uusitalo, H., Juuti-Uusitalo, K. & Skottman, H. (2014). Structure and barrier properties of human embryonic stem cell-derived retinal pigment epithelial cells are affected by extracellular matrix protein coating, *Tissue engineering. Part A*, Vol. 20(3-4), pp. 622-634.

Soubrane, G. & Coscas, G. (2013). Chapter 30 - Pathogenesis of Serous Detachment of the Retina and Pigment Epithelium, in: Ryan, S.J. et al. (ed.), *Retina (Fifth Edition)*, W.B. Saunders, London, pp. 618-623.

Stenzel, M.H., Barner-Kowollik, C. & Davis, T.P. (2006). Formation of honeycomb-structured, porous films via breath figures with different polymer architectures, *Journal of Polymer Science Part A: Polymer Chemistry*, Vol. 44(8), pp. 2363-2375.

Stern, J.H. & Temple, S. (2011). Stem cells for retinal replacement therapy. *Neurotherapeutics*, Vol. 8 pp. 736-743.

Strauss, O. (2005). The Retinal Pigment Epithelium in Visual Function, *Physiological Reviews*, Vol. 85(3), pp. 845-881.

Subrizi, A., Hiidenmaa, H., Ilmarinen, T., Nymark, S., Dubruel, P., Uusitalo, H., Yliperttula, M., Urtti, A. & Skottman, H. (2012). Generation of hESC-derived retinal pigment epithelium on biopolymer coated polyimide membranes, *Biomaterials*, Vol. 33(32), pp. 8047-8054.

Sumita, R. (1961). The Fine Structure of Bruch's Membrane of the Human Choroid as Revealed by Electron Microscopy, *Journal of Electron Microscopy*, Vol. 10(2), pp. 111-118.

Tallawi, M., Rosellini, E., Barbani, N., Cascone, M.G., Rai, R., Saint-Pierre, G. & Boccacini, A.R. (2015). Strategies for the chemical and biological functionalization of scaffolds for cardiac tissue engineering: a review, *Journal of the Royal Society, Interface*, Vol. 12(108), pp. 20150254.

Tanaka, M., Takayama, A., Ito, E., Sunami, H., Yamamoto, S. & Shimomura, M. (2007). Effect of pore size of self-organized honeycomb-patterned polymer films on spreading, focal adhesion, proliferation, and function of endothelial cells, *Journal of nanoscience and nanotechnology*, Vol. 7(3), pp. 763-772.

- Teymouri, S., Calejo, M.T., Hiltunen, M., Sorkio, A.E., Juuti-Uusitalo, K., Skottman, H. & Kellomäki, M. (2017). Collagen-immobilized polyimide membranes for retinal pigment epithelial cell adherence and proliferation, *Cogent Chemistry*, Vol. 3(1).
- Tezcaner, A., Bugra, K. & Hasırcı, V. (2003a). Retinal pigment epithelium cell culture on surface modified poly(hydroxybutyrate-co-hydroxyvalerate) thin films, *Biomaterials*, Vol. 24(25), pp. 4573-4583.
- Tezcaner, A., Bugra, K. & Hasırcı, V. (2003b). Retinal pigment epithelium cell culture on surface modified poly(hydroxybutyrate-co-hydroxyvalerate) thin films, *Biomaterials*, Vol. 24(25), pp. 4573-4583.
- Tezel, T.H. & Del Priore, L.V. (1997). Reattachment to a substrate prevents apoptosis of human retinal pigment epithelium, *Graefes archive for clinical and experimental ophthalmology = Albrecht von Graefes Archiv fur klinische und experimentelle Ophthalmologie*, Vol. 235(1), pp. 41-47.
- Thadavirul, N., Pavasant, P. & Supaphol, P. (2014). Development of polycaprolactone porous scaffolds by combining solvent casting, particulate leaching, and polymer leaching techniques for bone tissue engineering, *Journal of biomedical materials research. Part A*, Vol. 102(10), pp. 3379-3392.
- Thomson, J.A., Itskovitz-Eldor, J., Shapiro, S.S., Waknitz, M.A., Swiergiel, J.J., Marshall, V.S. & Jones, J.M. (1998). Embryonic stem cell lines derived from human blastocysts, *Science (New York, N.Y.)*, Vol. 282(5391), pp. 1145-1147.
- Tojkander, S., Gateva, G. & Lappalainen, P. (2012). Actin stress fibers – assembly, dynamics and biological roles, *Journal of cell science*, Vol. 125(8), pp. 1855-1864.
- Uppanan, P., Meesap, P., Thavornytikarn, B., Kosorn, W. & Janvikul, W. (2013). Study on Surface-Hydrolyzed Poly(butylene succinate)/Hydroxyapatite Composite Scaffolds for Cartilage Regeneration, *American Scientific Publishers*, Vol. 19(10), pp. 3070-3072.
- Vaajasaari, H., Ilmarinen, T., Juuti-Uusitalo, K., Rajala, K., Onnela, N., Narkilahti, S., Suuronen, R., Hyttinen, J., Uusitalo, H. & Skottman, H. (2011). Toward the defined and xeno-free differentiation of functional human pluripotent stem cell-derived retinal pigment epithelial cells, *Molecular vision*, Vol. 17 pp. 558-575.
- Wang, X., Ding, B. & Li, B. (2013). Biomimetic electrospun nanofibrous structures for tissue engineering, *Materials Today*, Vol. 16(6), pp. 229-241.
- Wheeldon, I., Farhadi, A., Bick, A.G., Jabbari, E. & Khademhosseini, A. (2011). Nanoscale tissue engineering: spatial control over cell-materials interactions, *Nanotechnology*, Vol. 22(21), pp. 212001.
- White, C., DiStefano, T. & Olabisi, R. (2017). The influence of substrate modulus on retinal pigment epithelial cells, *Journal of Biomedical Materials Research Part A*, Vol. 105(5), pp. 1260-1266.

- Wong, W.L., Su, X., Li, X., Cheung, C.M.G., Klein, R., Cheng, C. & Wong, T.Y. (2014). Global prevalence of age-related macular degeneration and disease burden projection for 2020 and 2040: a systematic review and meta-analysis, *The Lancet Global Health*, Vol. 2(2), pp. e116.
- Wu, Z., Zheng, K., Zhang, J., Tang, T., Guo, H., Boccaccini, A.R. & Wei, J. (2016). Effects of magnesium silicate on the mechanical properties, biocompatibility, bioactivity, degradability, and osteogenesis of poly(butylene succinate)-based composite scaffolds for bone repair, *Journal of Materials Chemistry B*, Vol. 4(48), pp. 7974-7988.
- Xiang, P., Wu, K., Zhu, Y., Xiang, L., Li, C., Chen, D., Chen, F., Xu, G., Wang, A., Li, M. & Jin, Z. (2014). A novel Bruch's membrane-mimetic electrospun substrate scaffold for human retinal pigment epithelium cells, *Biomaterials*, Vol. 35(37), pp. 9777-9788.
- Yamamoto, S., Tanaka, M., Sunami, H., Arai, K., Takayama, A., Yamashita, S., Morita, Y. & Shimomura, M. (2006). Relationship between adsorbed fibronectin and cell adhesion on a honeycomb-patterned film, *Surface Science*, Vol. 600(18), pp. 3785-3791.
- Zhang, Y. & Wang, C. (2007). Micropatterning of Proteins on 3D Porous Polymer Film Fabricated by Using the Breath-Figure Method, *Advanced Materials*, Vol. 19(7), pp. 913-916.
- Zhu, X., Chen, J., Scheideler, L., Altebaeumer, T., Geis-Gerstorfer, J. & Kern, D. (2004). Cellular Reactions of Osteoblasts to Micron- and Submicron-Scale Porous Structures of Titanium Surfaces, *Cells Tissues Organs*, Vol. 178(1), pp. 13-22.